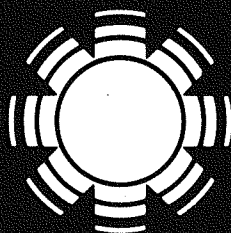


SERI/TA-253-2149
DE88012151

June 1988

Wind Loading on Solar Collectors

A. Shadit (University of Texas at El Paso)
L. M. Murphy (Solar Energy Research Institute)



SERI

Solar Energy Research Institute

A Division of Midwest Research Institute

1617 Cole Boulevard
Golden, Colorado 80401

SERI/TR-253-2169

C. 2

Operated for the

U.S. Department of Energy

under Contract No. DE-AC02-83CH10093

SOLAR ENERGY RESEARCH INSTITUTE
TECHNICAL LIBRARY

OCT 24 1985

GOLDEN, COLORADO 80401

SERI/TR-253-2169
UC Category: 62e
DE85012151

Wind Loading on Solar Collectors

S. Bhaduri (University of Texas at El Paso)
L. M. Murphy (Solar Energy Research Institute)

June 1985

Prepared under Task Nos. 1384.30 and 5102.31
FTP No. 463

Solar Energy Research Institute

A Division of Midwest Research Institute

1617 Cole Boulevard
Golden, Colorado 80401

Prepared for the
U.S. Department of Energy
Contract No. DE-AC02-83CH10093

PREFACE

The research and development described in this document was conducted within the U.S. Department of Energy's Solar Thermal Technology Program. The goal of the Solar Thermal Technology Program is to advance the engineering and scientific understanding of solar thermal technology and to establish the technology base from which private industry can develop solar thermal power production options for introduction into the competitive energy market.

Solar thermal technology concentrates the solar flux by means of tracking mirrors or lenses onto a receiver where the solar energy is absorbed as heat and converted into electricity or incorporated into products as process heat. The two primary solar thermal technologies, central receivers and distributed receivers, employ various point and line-focus optics to concentrate sunlight. Current central receiver systems use fields of heliostats (two-axis tracking mirrors) to focus the sun's radiant energy onto a single tower-mounted receiver. Parabolic dishes up to 17 meters in diameter track the sun in two axes and use mirrors or Fresnel lenses to focus radiant energy onto a receiver. Troughs and bowls are line-focus tracking reflectors that concentrate sunlight onto receiver tubes along their focal lines. Concentrated collector modules can be used alone or in a multimodule system. The concentrated radiant energy absorbed by the solar thermal receiver is transported to the conversion process by a circulating working fluid. Receiver temperatures range from 100°C in low-temperature troughs to over 1500°C in dish and central receiver systems.

The Solar Thermal Technology Program is directing efforts to advance and improve each system concept through the research and development of solar thermal materials, components, and subsystems, and the testing and performance evaluation of subsystems and systems. These efforts are carried out through the technical direction of DOE and its network of national laboratories that work with private industry. Together they have established a comprehensive, goal-directed program to improve performance and provide technically proven options for eventual incorporation into the nation's energy supply.

To be successful in contributing to an adequate national energy supply at reasonable cost, solar thermal energy must eventually be economically competitive with a variety of other energy sources. Components and system-level performance targets have been developed as quantitative program goals. The performance targets are used in planning research and development activities, measuring progress, assessing alternative technology options, and making optimal component developments. These targets will be pursued vigorously to insure a successful program.

This specific report addresses wind loading on solar collectors since the determination of wind loading is one of the major design considerations in designing tracking and field-mounted solar collectors. The main objective of the report is to review and assess the present design methodology for wind loading on collectors for solar thermal applications and to recommend areas of further investigation for developing realistic criteria to determine reliable and adequate wind loads. The feasibility of using innovative design considerations to reduce the magnitude of wind loads on the solar collectors is also

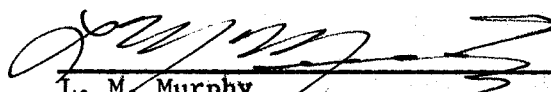
considered. This report contains valuable information regarding the comparative studies of various aspects of design methodology and should be of interest to design engineers and developers of solar collectors.

The authors would like to thank the numerous individuals at SERI who provided valuable discussions and support during the course of this study. In addition, the authors would like to thank those technologists outside of SERI who provided valuable comments and suggestions in their reviews of earlier drafts of this document; these are Bill Delemeter, Clayton Mavis, Jon Peterka, Jim Leonard, Martin Scheve, Frank Wilkins, Kenell Touryan, Jeff Shingleton, and Aharon Roy.

The first author extends his thanks and appreciation to the U.S. Department of Energy (DOE) and the American Society for Engineering Education (ASEE) for the opportunity to do this research at SERI. This area of research is supported by the DOE Solar Thermal Program under the direction of Frank Wilkins and Martin Scheve.





S. Bhaduri
University of Texas at El Paso


L. M. Murphy
Solar Energy Research Institute

Approved for

SOLAR ENERGY RESEARCH INSTITUTE


John Thornton, Manager
Thermal Systems and Engineering Branch


L. J. Shannon, Director
Solar Heat Research Division

SUMMARY

Objective

The objective is to review and assess the present methodology for predicting and designing for wind loading on solar collectors for trough, dish, and heliostat applications and possibly for large field-mounted photovoltaic arrays. Another objective is to recommend areas of further investigation for developing realistic criteria to adequately determine the wind loads on these structures.

Discussion

The present method of determining the wind load, using the code ANSI A58.1-1982 of the American National Standard Institute, is overly conservative. The recent model studies of solar collectors in boundary layer wind tunnels under simulated atmospheric flow conditions yielded valuable information regarding the wind forces on the collectors and established various dimensionless force and moment coefficients corresponding to the mean wind velocities and their direction of approach. A significant amount of model testing was devoted to studies involving both individual collectors and fields of collectors. The effects of porous fences or barriers at the edge of the collector field and the shielding effects of the adjacent collectors in the field in reducing the effective wind loads on the collectors were also studied in the wind tunnels at various test facilities. The results of these studies indicate that the wind load can be reduced considerably even beyond the levels that trough designers have already used.

Conclusions and Recommendations

In this study, the following were accomplished:

- Development of elevation-dependent longitudinal velocity profiles for various exposure conditions.
- Comparative study of the total force coefficient of a flat plate of various aspect ratios and at various angles of attack. Values obtained for the ANSI A58.1-1982 code, ASCE Task Comm. 1961 [23], and full-scale heliostat tests were used for the comparison.
- Comparative study of the spectra of longitudinal, vertical, and lateral velocity fluctuations. Spectra for the velocity fluctuations for frequency range 0.001-10.0 Hz were calculated and compared graphically. The spectra used for the Building Code ANSI A58.1-1982 and the spectra in Kaimal et al. [26] were considered.
- Estimation of the resultant angle of attack (relative to the horizontal) of the turbulent wind field for various exposures such as open field and suburban location. This is particularly important when considering heliostats in the stowed position. The angle of attack due to turbulent fluctuating velocity is strongly dependent on the roughness parameter of the flow field. For a roughness element of 0.123 m (0.4 ft) in a

suburban area, and wind speeds of 30 mph, 50 mph, and 90 mph at an elevation of 10 m (32.8 ft), the angles of attack due to fluctuating vertical velocity are 4.68° , 4.60° , and 4.30° , respectively.

Recommendations for further studies that might reduce the wind loading on the collector are to

- Modify the flow locally by using a turbulence stimulator in the form of porous eaves around the heliostat to discourage the flow separation at the edges of the heliostat
- Determine experimentally the appropriate air gap between the modules to encourage ventilation around the module
- Study the effects of perimeter fences and fences in the field around a group of heliostat zones to reduce the overall wind load
- Determine the magnitude of wind speed and its direction by developing a wind rose for the heliostat field. A physical scale model of this heliostat field may be tested in the atmospheric wind tunnel to obtain information regarding the wind speed, its direction, and turbulent characteristics.

TABLE OF CONTENTS

	<u>Page</u>
1.0 Introduction.....	1
2.0 Estimates of Wind Forces.....	5
2.1 Atmospheric Turbulence Spectra.....	19
2.2 Variation of Wind Angle from the Horizontal.....	23
3.0 Reduction of Wind Loading.....	29
4.0 Conclusion and Recommendations.....	32
5.0 References.....	34

LIST OF FIGURES

	<u>Page</u>
2-1 Distribution of Gradient Wind for Various Exposures.....	9
2-2 Variation of Wind Speed with Elevation, $(U_{30})_C = 27$ mph.....	14
2-3 Variation of Wind Speed with Elevation, $(U_{30})_C = 50$ mph.....	14
2-4 Variation of Wind Speed with Elevation, $(U_{30})_C = 70$ mph.....	15
2-5 Variation of Wind Speed with Elevation, $(U_{30})_C = 90$ mph.....	15
2-6 Variation of Velocity Pressure with Wind Velocity.....	16
2-7 A Geometry for Flow past a Flat Plate.....	17
2-8 Variation of Force Coefficient with Angle of Attack, Aspect Ratio, $\lambda = 1.0$	18
2-9 Variation of Force Coefficient with Angle of Attack, Aspect Ratio, $\lambda = 3.0$	19
2-10 Longitudinal Turbulence Spectra, $U = 44.73$ mph.....	22
2-11 Turbulent Wind Spectra, $U = 44.73$ mph.....	22
2-12 Turbulent Wind Spectra, $U = 90.0$ mph.....	23
2-13 Strong Wind Velocity Spectra of Daniels.....	24
2-14 Peak Angle of Attack due to Turbulent Lateral Velocity.....	27
2-15 Peak Angle of Attack due to Turbulent Vertical Velocity.....	28

LIST OF TABLES

	<u>Page</u>
2-1 Gradient Wind.....	8
2-2 Variation of Wind Velocity with Height, $U_{30} = 27.0$ mph.....	10
2-3 Variation of Wind Velocity with Height, $U_{30} = 50.0$ mph.....	11
2-4 Variation of Wind Velocity with Height, $U_{30} = 70.0$ mph.....	12
2-5 Variation of Wind Velocity with Height, $U_{30} = 90.0$ mph.....	13
2-6 Velocity Pressure.....	16
2-7 Force Coefficient C_f for Flow past a Flat Plate, Aspect Ratio, $\lambda = 1.0$	17
2-8 Force Coefficient C_f for Flow past a Flat Plate, Aspect Ratio, $\lambda = 3.0$	18
2-9 Dimensionless Constants for Longitudinal and Lateral Turbulence Spectra.....	25
2-10 Variation of Angle of Attack due to Fluctuating Lateral Velocity....	26
2-11 Variation of Angle of Attack due to Fluctuating Vertical Velocity.....	27

NOMENCLATURE

A,B,C,D	basic exposure categories
A	characteristic surface area of collector, m^2 (ft^2)
C_f	force coefficient, dimensionless
C_M	moment coefficient, dimensionless
F	wind force, N (lbf)
F_D	drag force, N (lbf)
F_L	lift force, N (lbf)
f	Monin coordinate, dimensionless
G_h	gust response factor at height $z = h$, dimensionless
K_z	velocity pressure exposure coefficient at height z
L	moment arm length, m (ft)
M	moment of a force, N m (lbf ft)
n	frequency, Hz
q	dynamic pressure, N/m^2 (lb/ft^2)
q_z	velocity pressure evaluated at height z , N/m^2 (lb/ft^2)
$S(z,n)$	spectrum of longitudinal velocity fluctuations, N m/n (lbf ft s)
$S_w(z,n)$	spectrum of vertical velocity fluctuations, N m/n (lbf ft s)
$S_v(z,n)$	spectrum of lateral velocity fluctuations, N m/n (lbf ft s)
$U(z)$	mean velocity at height z
U_g	longitudinal component of velocity at gradient height z_g
U_z	longitudinal component of velocity at height z
U_*	friction velocity, m/s (ft/s)
V	basic wind velocity, m/s (mph)
z	vertical elevation, m (ft)
z_c	reference height of ANSI code, m (ft)
z_g	gradient height, m (ft)
z_r	reference height, m (ft)
α	angle of attack, degree
β	coefficient $(z/z_r)^{c5}$
λ	aspect ratio
ρ	mass density, kg/m^3 (slug/ ft^3)
ϕ	stability parameter
ω	frequency, H_z

SECTION 1.0

INTRODUCTION

During the last two decades, there have been a number of significant developments in the meteorological aspects of the wind-loading problem. Advances in structural designs, particularly for high-rise structures, required accurate and more reliable meteorological information about the wind-loading processes. Various research results and histories of failures of structures [1] indicate the damaging effects of repeated wind-induced loads on structures. Efforts have been made to design structures that resist the repeated loading action of wind [2,3]. This contradicts the more conventional design approach, which is mainly concerned with static application of a single large load derived from the guidelines furnished by the National Building Codes. Experience suggests that unserviceability due to repeated loading effects is a more likely occurrence than unserviceability or collapse from a single application of an exceptionally large load [4]. The common types of structural unserviceability caused by repeated wind loading are (1) fatigue failure, (2) foundation settlement, (3) excessive deflection, and (4) induced motion of unacceptable level. Fatigue failure is an important design consideration even for the design of low-rise structures. Examples of fatigue failure due to wind are found in structures such as towers, lamp standards, chimney stacks, and even bridges [5]. As innovative concentrator designs become less robust to reduce the amount of materials and costs required, all of these issues become more of a concern. An example of such a lightweight concentrator is the stretched-membrane heliostat.

Wind is one of the principal loads acting on above-ground engineering structures. An accurate determination of wind loading is a fundamental design consideration in deciding what degree of safety and economy can be achieved in such a structure. It is common practice to design structures to resist the highest wind to which they may be subjected. The highest wind is determined from the analysis of extreme value statistics of recorded wind velocities for a long period of time for a particular region.

The wind loads are considered in terms of a steady applied force, independent of the structure's shape, size, and dynamic characteristics, and a coefficient denoting the amplification that can arise through the interaction of the superimposed pressure fluctuations and the structure's dynamic response. The reliable estimate of this coefficient is quite involved and requires detailed knowledge of the site-specific wind climatology. The wind speeds used in current design specification are based on the U.S. Weather Bureau observation of the "fastest mile"* of wind (from distribution of extreme wind in the United States) multiplied by a gust factor to allow for the fluctuations in the wind speed. The gust response factor is a measure of the effective dynamic load produced by the gusts and is intended to translate the dynamic responses produced by the gust loading into simpler static design criteria. Although this

*"Fastest mile" corresponds to the highest (extreme) wind speed in miles per hour, measured at a standard height of 33 ft above the ground level in an open-country location.

approach has often resulted in a safe, conservative estimate of wind loading, the neglect of the dynamic properties and size of the structure, the surface roughness, local obstructions, and the wind directions and their frequencies inherent in applying the fastest mile of wind could result in unsafe structures or in costly overdesigns.

Vellozzi and Cohen [6] developed a design methodology based on a power spectrum analysis of the dynamic structural response of a simple linear single degree of freedom system with viscous damping and reported measurements of wind gust spectra and gust correlation coefficients. The results of the analysis are presented in equations and charts that permit us to determine the gust response factors for buildings and conventional structures. However, for structures like solar collectors, the method is not satisfactory since it does not account for the effects of surface roughness, terrain characteristics, and directional distribution of wind. We still do not understand the mechanism whereby gust pressure is induced on ground-based structures. Moreover, these design guidelines are applicable only to the situations where the principal wind loading is drag. Lateral and vertical wind components normal to the gross flow direction and gustiness are not considered.

Davenport [7] used a statistical approach to estimate the mean gradient wind speed that has a specified return period or probability of exceeding on the basis of the mode and dispersion factor for the extreme gradient wind speed field at the site of the structure. This method may be used to determine the mean wind speed at some specific height above the ground if a reliable estimate of ground roughness and exposure of the site is available. The ground roughness is the principal parameter governing the mean wind speed profile and gustiness. Knowing the mean wind speed at the structure height corresponding to the gradient speed and the ground roughness, we can define the vertical and horizontal gust spectra. Davenport based his estimate of the gust force superimposed on the mean wind forces on the lateral gust spectra.

In his pioneering paper, Davenport [7] outlined the rationale for determining the design wind velocities. Briefly, he considered the extreme value statistics of the site, specific wind velocity, local ground roughness and exposure characteristics, wind direction rosettes, and a weighting parameter. The methodology outlines the determination of the basic design wind velocity that corresponds to the extreme sustained wind velocity giving rise to the steady component of the pressure. This velocity is essentially an average velocity, and the determination of a suitable averaging interval is an important feature of the method. Davenport attempts to process the records from a wide variety of anemometers of differing exposures and periods of records and to determine statistically how the records may be related to one another. This minimizes the systematic errors that may arise in the records because of uncontrolled anemometer siting and improves the records' overall reliability. The influence of the local surface roughness on both the magnitude of surface velocities and the increase of velocity with height is very important. Combining these results with extreme value statistics [8] leads to a qualitative method through which basic design wind velocities of a given probability of occurrence may be predicted for locations of differing surface roughness.

Thom [9] introduced the concept of the annual fastest mile wind speed as the best available measure of wind speed for design purposes. The physical model for the boundary shear layer was assumed to have a standard level of 9.14 m (30 ft) and a velocity profile using a $1/7$ power law. Computational methods were developed for fitting the Fisher-Tippett Type II extreme value distribution [10], which fitted the data well. The methods developed [9] were applied to the airport and open-country data series for 138 stations; maps were drawn for the 2-year, 50-year, and 100-year mean recurrence intervals. These maps received general acceptance as the U.S. standards. The methods of determining other quantities, such as probabilities for a fixed period and confidence limits for the estimates obtained from the maps, were given.

In his subsequent paper, Thom [11] observed that the distribution of the logarithm of a Fisher-Tippett Type II (Frechet) distribution [5] is a logarithmic transformation of the Type I distribution. Although this fact was not used in the previous paper, further examination of the extensive non-extreme wind data showed that such data follow a log normal distribution closely, which would indicate a Type I distribution for the extreme of the logarithm. This also substantiates the validity of the choice of the Frechet distribution for extreme winds. The maps developed by Thom [11] in which the Type I distribution is fit by order statistics to 150 stations were used extensively as the ANSI standard for building codes of the United States. The maps depicted the isotech lines in miles per hour of the annual extreme mile, 10.0 m (33 ft) above the ground, for 2-year, 10-year, 25-year, 50-year, and 100-year mean recurrence intervals.

The basic wind speeds used to determine the design wind loads on buildings and other structures are given in Figure 1 of the ANSI A58.1-1982 code [12] for the contiguous United States and Alaska and in Table 7 for Hawaii and Puerto Rico. Special considerations are allowed for those regions for which records or experience indicate that the wind speeds are lighter than those indicated in Figure 1 and Table 7 of the code [12]. The ANSI A58.1-1982 code also allows estimation of the basic wind speed based on regional climatic data and extreme value statistical analysis; however, the basic wind speed must be at least 70 mph.

All investigators recognize the qualitative nature of the idealized isotech lines based on data collected under diverse conditions and suggest that they be used with great care in determining the wind load for a specific structure in a specific site. Often, the probability of exceeding a particular wind velocity for a certain recurrence interval is related to the degree of risk associated with the lifetime of the structure. The probability that a structure will be subjected to a magnitude of wind loading is not site specific since wind data do not reflect the true nature of wind distribution at the site in question. The ground roughness, the exposure features, wind direction, and terrain conditions are not included in the methodology used by the codes.

The American National Standard A58.1-1982 [12] contains a definition of design wind speed in terms of the mean recurrence interval or return period. For a mean recurrence interval, the corresponding design wind speed is calculated from the expression of the cumulative distribution function of the extreme wind. The parameters of this function are estimated from the data of the

largest wind speed for every year on record. The mean recurrence interval to be used in the design is selected as a function of "intended operational usage, anticipated life of the structure, degree of sensitivity to wind and the risk of loss of human life and property in case of failure" [12]. Implicit in the selection of the mean recurrence interval is the assumption that a given recurrence interval will ensure the same level of safety for any two structures subjected to wind loads provided that the reliability of the two structures is equal. Simiu [13] examined the validity of this simplified assumption and showed conclusively that the use of design wind maps based on the standard mean recurrence interval does not ensure a consistent level of safety for structures subjected to wind loads. Simiu emphasized that extensive research is required to develop regional and site-specific wind speed provisions based on a reliability consideration.

Because of the uncertainty and qualitative nature of the methodology used to estimate wind loading on structures, it seems reasonable to obtain the design parameters from simulation studies of sites under various wind speeds and wind directions. Various simulated experimental studies in the wind tunnels have already yielded valuable information.

Murphy [14] reviewed the existing methodologies for estimating the wind loading on solar collectors. He summarized 33 studies relevant to wind loading on solar collectors, heliostats, and photovoltaic arrays. The report, which contains valuable information regarding the present state of the art, has been used as a guide for this study.

Roschke [15] examined the problems and complications arising from wind loading on solar concentrators. He emphasized the site-specific nature of wind loading with associated important bearing on the design, cost, performance, operation and maintenance, safety, survival, and replacement of solar collectors, particularly the paraboloidal concentrators.

The primary objective of this study is to review and assess the present design methodology on wind loading on solar collectors, particularly the heliostats, and to recommend areas of further investigation to define realistic criteria for determining adequate wind loads. The model testing of the solar collectors in the environmental wind tunnels [16,17] indicates that it is possible to reduce the wind load considerably. In view of the feasibility of load reduction, we compare studies of the total force coefficient of a flat plate of various aspect ratios and at various angles of attack and studies of the spectra of longitudinal, vertical, and lateral velocity fluctuations. The angles of attack of the turbulent wind to the horizontally placed flat plate are important because of their effects on the net moment of the structure. We attempt to estimate the magnitude of angles from turbulent spectrum analysis.

This study does not consider the wind-loading effects caused by turbulence; i.e., (1) buffeting, (2) vortex shedding forces produced by the structure's own wake acting on the afterbody of the structure behind the separation point, and (3) aeroelastic forces induced by the oscillating motion of the structure.

SECTION 2.0

ESTIMATES OF WIND FORCES

The wind load on the low-height structures, such as heliostats extending over a large land area, is a major design consideration. Properly determining the wind loads on the heliostats is essential for realistic structural designs and cost estimates. The ANSI A58.1-1982 code [12] is commonly used as a design guide. The code is primarily developed for buildings and other structures. Generally, estimates are made, in the absence of more reliable experimental values obtained from model study, by considering the heliostats as other structures.

The wind force F on a structure is given by

$$F = q_z G_h C_f A_p , \quad (2-1)$$

where

q_z = velocity pressure evaluated at height z above ground (lb/ft^2)*

G_h = gust response factor at height $z = h$

C_f = force coefficient

A_p = projected area normal to wind.

The velocity pressure q_z is calculated from the standard formula [12]

$$q_z = 0.00256 K_z V^2 , \quad (2-2)$$

where

K_z = velocity pressure exposure coefficient at height z

V = basic wind speed (mph).

The values of the various coefficients and factors are taken from the tables provided in the code for various exposures of the site of the structure. An exposure category is determined for the site at which the structure is situated. It reflects the characteristics of ground surface irregularities. Generally, four basic exposure categories are considered. Exposures A, B, C, and D represent the large city center, urban and suburban areas, open terrain, and flat, unobstructed coastal areas, respectively.

*Since the standards and codes used for comparative assessments are described in their original form using English units, SI units will follow the English equivalents.

The structure is designed for the environmental conditions with specified wind speed and mean recurrence interval. Generally, operating environmental conditions and extreme environmental conditions with assumed mean recurrence interval and expected life of the structure are considered to estimate the probability of exceeding the maximum design wind velocity. The probability is derived from the consideration of the extreme value ordered statistics of Thom [9]. The probability of exceeding the design velocity, or risk of occurrence as it is called, is not based on site-specific extreme wind records. The recorded wind data at the airport of a relatively large city may not be applicable to a smaller suburban city 50 miles away with different terrain features. In fact Simiu [13], Davenport [7], and McDonald [18] have questioned the validity of the basic assumptions and simplified methodology.

The variation of longitudinal component of wind velocity with elevation in the earth's lower atmosphere is expressed by

$$U_z = U_g \left(\frac{z}{z_g} \right)^n, \quad (2-3)$$

where

U_z = longitudinal component of velocity at height z

U_g = longitudinal component of velocity at gradient height z_g

n = an exponent.

The following analytical relations of the velocity profiles relative to the velocity U_{30} at a height equal to 30 ft have been derived for ready reference.

$$\text{Exposure C: } z_g = 900.0 \text{ ft} \quad n = 0.1429 \quad (2-4)$$

$$U_z = U_{30} \left(\frac{z}{30} \right)^{0.1429}$$

$$\text{Exposure B: } z_g = 1200.0 \text{ ft} \quad n = 0.2222 \quad (2-5)$$

$$U_z = U_{30} \left(\frac{z}{30} \right)^{0.2222}$$

$$\text{Exposure A: } z_g = 1500.0 \text{ ft} \quad n = 0.3333 \quad (2-6)$$

$$U_z = U_{30} \left(\frac{z}{30} \right)^{0.3333}$$

The longitudinal components of wind velocity at elevation $z = 30$ ft for the exposure conditions A, B, and C are related by

$$(U_{30})_B = 0.7163(U_{30})_C \quad (2-7a)$$

and

$$(U_{30})_A = 0.4414(U_{30})_C \quad (2-7b)$$

Table 2-1 shows the distribution of gradient wind for various exposures. Figure 2-1 graphically shows the dimensionless gradient wind distribution with elevation for the exposures of A, B, and C. Tables 2-2 through 2-5 give the values of the velocity variation with height for reference velocities of 27.0 mph, 50.0 mph, 70.0 mph, and 90.0 mph, respectively. Figures 2-2 through 2-5 show the variations of wind speed with elevation for the exposures. $(U_{30})_C$ is the velocity of wind at an elevation $z = 30$ ft for exposure category C. Table 2-6 gives the computed values of velocity pressure obtained from the formula $q_z = 0.00256 V^2$. Figure 2-6 shows the variation of velocity pressure with wind velocity.

In recent years, the model studies of structures in simulated flow fields have yielded more reliable wind-load design values expressed in terms of dimensionless force and moment coefficients. The aerodynamics of structures in turbulent shear flows of the earth's lower atmosphere involve nonlinear interaction of the turbulent approach--flow with highly complex turbulent boundary layers and subsequent boundary layer separation and turbulent wake formation. Cermak [19] and Bhaduri [20] showed the feasibility of simulating the earth's boundary layers in the properly designed wind tunnel. Lindsay [21], Randall et al. [22], Peglow [16], and Xerikos et al. [17] tested the models of the solar collectors, heliostats, and heliostat arrays in the environmental wind tunnels and presented useful experimental results that could be used for determining design wind loads.

Based on the principle of similitude in model studies, the equality of the force and moment coefficients for the model and for the prototype, respectively, is well established. The force coefficient C_f is defined by

$$C_f = \frac{F}{qA_p}, \quad (2-8)$$

where

F = resultant force acting on the structure

q = dynamic pressure, often called velocity pressure

A_p = projected area normal to wind.

The moment coefficient C_M is defined by

$$C_M = \frac{M}{qA_p L}, \quad (2-9)$$

where

M = moment of the total force about a reference point

L = a characteristic moment arm length.

The dynamic pressure q is expressed by

$$q = \frac{1}{2} \rho U^2, \quad (2-10)$$

Table 2-1. Gradient Wind

z (ft)	C		B		A	
	$z_g = 900 \text{ ft}$ (274.32 m)		$z_g = 1200 \text{ ft}$ (365.76 m)		$z_g = 1500 \text{ ft}$ (457.20 m)	
	z/z_g	U/U_g	z/z_g	U/U_g	z/z_g	U/U_g
0	0	0	0	0	0	0
15	0.017	0.557	0.013	0.378	0.010	0.215
30	0.033	0.615	0.025	0.441	0.020	0.271
40	0.044	0.641	0.033	0.470	0.027	0.299
50	0.056	0.662	0.042	0.494	0.033	0.322
75	0.083	0.701	0.063	0.540	0.050	0.368
100	0.111	0.731	0.083	0.576	0.067	0.406
200	0.222	0.807	0.167	0.672	0.133	0.511
300	0.333	0.855	0.250	0.735	0.200	0.585
400	0.444	0.891	0.333	0.783	0.267	0.644
500	0.555	0.919	0.417	0.823	0.333	0.693
600	0.667	0.944	0.500	0.857	0.400	0.737
700	0.778	0.965	0.583	0.887	0.467	0.776
800	0.889	0.983	0.667	0.914	0.533	0.811
900	1.000	1.000	0.750	0.938	0.600	0.843
1000			0.833	0.960	0.667	0.874
1100			0.917	0.981	0.733	0.902
1200			1.000	1.000	0.800	0.928
1300					0.867	0.953
1400					0.933	0.977
1500					1.000	1.000

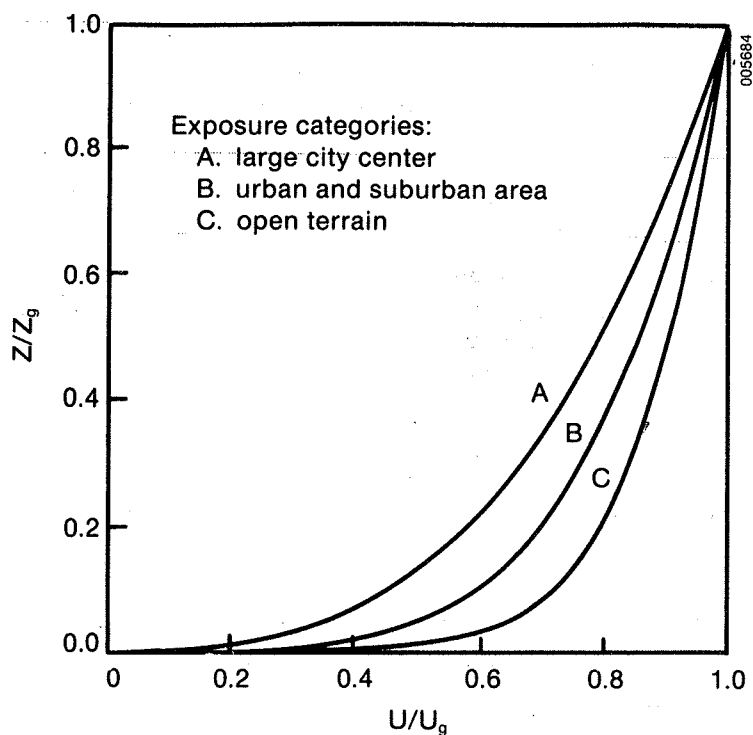


Figure 2-1. Distribution of Gradient Wind for Various Exposures

where

ρ = mass density of air

U = mean approach velocity.

The wind effects can be resolved into two force components--drag force F_D and lift force F_L . They are expressed as

$$F_D = C_D q A_p, \quad (2-11)$$

where

C_D = drag coefficient

A_p = projected area normal to the wind;

and

$$F_L = C_L q A_p, \quad (2-12)$$

where

C_L = lift coefficient.

From the vector nature of the force and its components, it can be shown that

$$F = (F_D^2 + F_L^2)^{1/2}, \quad (2-13)$$



Table 2-2. Variation of Wind Velocity with Height,
 $U_{30} = 27 \text{ mph (12 m/s)}$

Elevation (ft) ^a	Exposure C		Exposure B		Exposure A	
	Wind Speed V (mph) ^b	Velocity Pressure q (lb/ft ²) ^c	Wind Speed V (mph)	Velocity Pressure q (lb/ft ²)	Wind Speed V (mph)	Velocity Pressure q (lb/ft ²)
0	0	0	0	0	0	0
10	23.1	1.37	15.2	0.59	8.3	0.18
15	24.6	1.55	16.6	0.71	9.5	0.23
20	25.6	1.68	17.7	0.80	10.4	0.28
25	26.4	1.78	18.6	0.89	11.2	0.32
30	27.0	1.87	19.4	0.96	12.0	0.37
40	28.20	2.04	20.7	1.10	13.2	0.45
50	29.2	2.18	21.7	1.21	14.2	0.52
75	30.86	2.44	23.8	1.46	16.2	0.67
100	32.2	2.65	25.3	1.64	17.9	0.82
150	34.1	2.98	27.7	1.96	20.4	1.07
200	35.4	3.21	29.6	2.24	22.5	1.30
300	37.6	3.62	32.3	2.67	25.7	1.69
500	40.2	4.14	36.2	3.35	30.50	2.38
700	42.4	4.60	39.0	3.89	34.1	2.98
900	44.0	4.96	41.28	4.36	37.1	3.52
1000			42.3	4.58	38.5	3.79
1100			43.2	4.78	39.7	4.03
1200			44.0	4.96	40.9	4.28
1300					42.0	4.52
1400					43.0	4.73
1500					44.0	4.96

^aTo convert to m, multiply by 0.3048.

^bTo convert to m/s, multiply by 0.447.

^cTo convert to Pa, multiply by 47.88.

Table 2-3. Variation of Wind Velocity with Height,
 $U_{30} = 50 \text{ mph (22 m/s)}$

Elevation (ft) ^a	Exposure C		Exposure B		Exposure A	
	Wind Speed V (mph) ^b	Velocity Pressure p (lb/ft ²) ^c	Wind Speed V (mph)	Velocity Pressure q (lb/ft ²)	Wind Speed V (mph)	Velocity Pressure q (lb/ft ²)
0	0	0	0	0	0	0
10	42.8	4.69	28.1	2.02	15.3	0.60
15	45.4	5.28	30.8	2.43	17.6	0.79
20	47.3	5.73	32.8	2.75	19.3	0.95
25	48.8	6.10	34.5	3.05	20.8	1.11
30	50.0	6.40	35.9	3.30	22.1	1.25
40	52.2	6.98	38.30	3.76	24.40	1.52
50	53.9	7.44	40.2	4.14	26.2	1.76
75	57.1	8.35	44.0	4.96	30.0	2.30
100	59.5	9.06	46.9	5.63	33.1	2.80
200	65.7	11.05	54.7	7.66	41.6	4.43
500	74.9	14.36	67.1	11.53	56.5	8.17
700	78.6	15.82	72.3	13.38	63.2	10.23
900	81.5	17.00	76.5	14.90	68.7	12.08
1200			81.5	17.00	75.7	14.67
1500					81.5	17.00

^aTo convert to m, multiply by 0.3048.

^bTo convert to m/s, multiply by 0.447.

^cTo convert to Pa, multiply by 47.88.

and

$$C_f = (C_D^2 + C_L^2)^{1/2} \quad (2-14)$$

To compare the values of C_f obtained by using the guidelines of the ANSI A58.1-1982 code with the values obtained by using the methodology of the ASCE Task Committee of 1961 [23], flows past vertical plates with aspect ratios, $\lambda = (\text{width/height})$, of 3 and 1 are considered (see Figure 2-7). The experimental results of Peglow's [16] full-scale test of a heliostat of aspect ratio $\lambda = 1.0$ are also used for the comparison. For angles of attack of 0° - 30° , the corresponding values of force coefficient C_f are taken from Table 11 of ANSI A58.1-1982 code [12] and Figure 5(d) of Paper 3269 of the

Table 2-4. Variation of Wind Velocity with Height,
 $U_{30} = 70 \text{ mph (31 m/s)}$

Elevation (ft) ^a	Exposure C		Exposure B		Exposure A	
	Wind Speed V (mph) ^b	Velocity Pressure p (lb/ft ²) ^c	Wind Speed V (mph)	Velocity Pressure q (lb/ft ²)	Wind Speed V (mph)	Velocity Pressure q (lb/ft ²)
0	0	0	0	0	0	0
10	59.8	9.15	39.3	3.95	21.4	1.17
15	63.4	10.29	43.0	4.73	24.5	1.56
20	66.1	11.19	45.8	5.37	27.0	1.87
30	70.0	12.54	50.1	6.43	30.90	2.44
50	75.3	14.52	56.2	8.09	36.6	3.43
100	83.1	17.68	65.5	10.98	46.2	5.46
200	91.8	21.57	76.4	14.94	58.2	8.67
300	97.3	24.24	83.6	17.89	66.60	11.36
400	101.4	26.32	89.2	20.37	73.3	13.75
500	104.6	28.01	93.7	22.48	79.0	15.98
600	107.4	29.53	97.6	24.39	83.9	18.02
700	109.8	30.86	100.9	26.06	88.3	19.96
800	111.9	32.06	104.0	27.69	92.3	21.81
900	113.8	33.15	106.8	29.20	96.0	23.59
1000			109.3	30.58	99.4	25.29
1100			111.6	31.88	102.6	26.95
1200			113.8	33.15	105.7	28.60
1300					108.5	30.14
1400					111.2	31.66
1500					113.8	33.15

^aTo convert to m, multiply by 0.3048.

^bTo convert to m/s, multiply by 0.447.

^cTo convert to Pa, multiply by 47.88.

Table 2-5. Variation of Wind Velocity with Height,
 $U_{30} = 90 \text{ mph (40 m/s)}$

Elevation (ft) ^a	Exposure C		Exposure B		Exposure A	
	Wind Speed V (mph) ^b	Velocity Pressure q (lb/ft ²) ^c	Wind Speed V (mph)	Velocity Pressure q (lb/ft ²)	Wind Speed V (mph)	Velocity Pressure q (lb/ft ²)
0	0	0	0	0	0	0
10	77.0	15.18	50.5	6.53	27.5	1.94
15	81.6	17.05	55.3	7.83	31.5	2.54
20	85.0	18.05	58.9	8.88	34.7	3.08
25	87.7	19.69	61.9	9.81	37.4	3.58
30	90.0	20.74	64.5	10.65	39.7	4.03
40	93.8	22.52	68.7	12.08	43.7	4.89
50	96.1	23.64	72.2	13.34	47.1	5.68
75	102.6	26.95	79.0	15.98	53.9	7.44
100	106.9	29.25	84.2	18.15	59.3	9.00
200	118.0	35.65	98.3	24.74	74.8	14.32
500	134.5	46.31	120.5	37.17	101.5	26.37
700	141.2	51.04	129.8	43.25	113.5	32.98
900	146.3	54.79	137.3	48.26	123.4	38.98
1200			146.3	54.79	135.8	47.21
1500					146.3	54.79

^aTo convert to m, multiply by 0.3048.

^bTo convert to m/s, multiply by 0.447.

^cTo convert to Pa, multiply by 47.88.

Task Committee (TC) [23]. The results are shown in Tables 2-7 and 2-8. They are also presented graphically in Figures 2-8 and 2-9.

The ratios of C_f (code)/ C_f (TC) and C_f (code)/ C_f (heliostat) indicate that the code values, within the range of the angles of attack, are generally 10% to 25% higher for $\lambda = 1.0$. For $\lambda = 3.0$, they are 22% to 25% higher. Thus the code gives an overestimate of the wind loads for the flow past an inclined flat plate. The values of C_f estimated by using the Task Committee guidelines compare favorably with the experimental results of the full-scale heliostat testing. Figures 2-8 and 2-9 show that the ANSI coefficient C_f is moderately conservative if the angle of attack is less than 15° and that it is somewhat more conservative at higher angles of attack. For longer plates, the code values are generally more conservative.

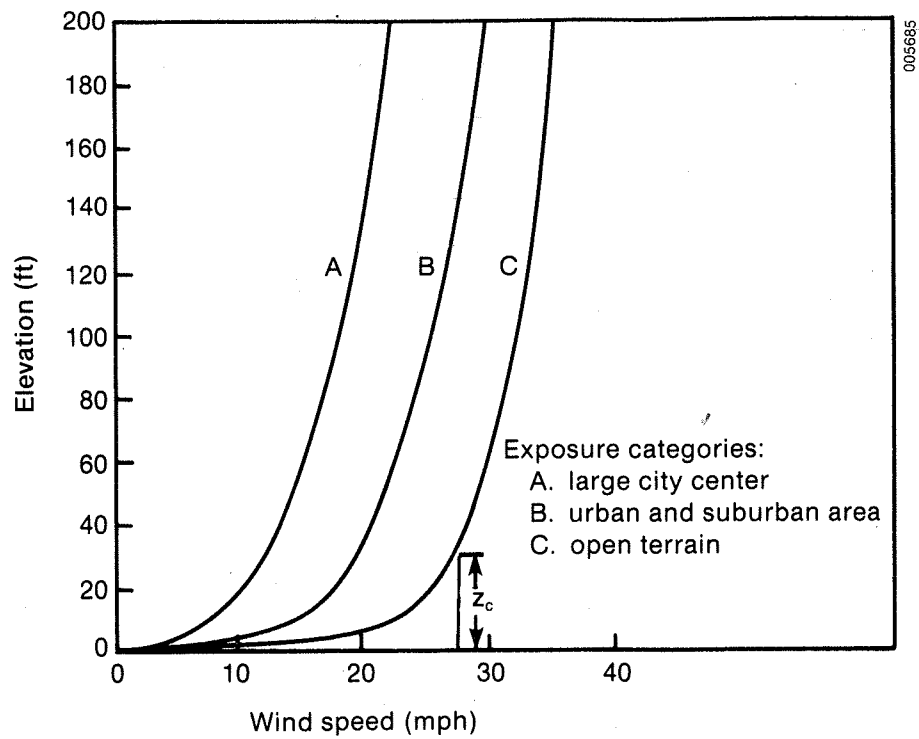


Figure 2-2. Variation of Wind Speed with Elevation, $(U_{30})_C = 27$ mph

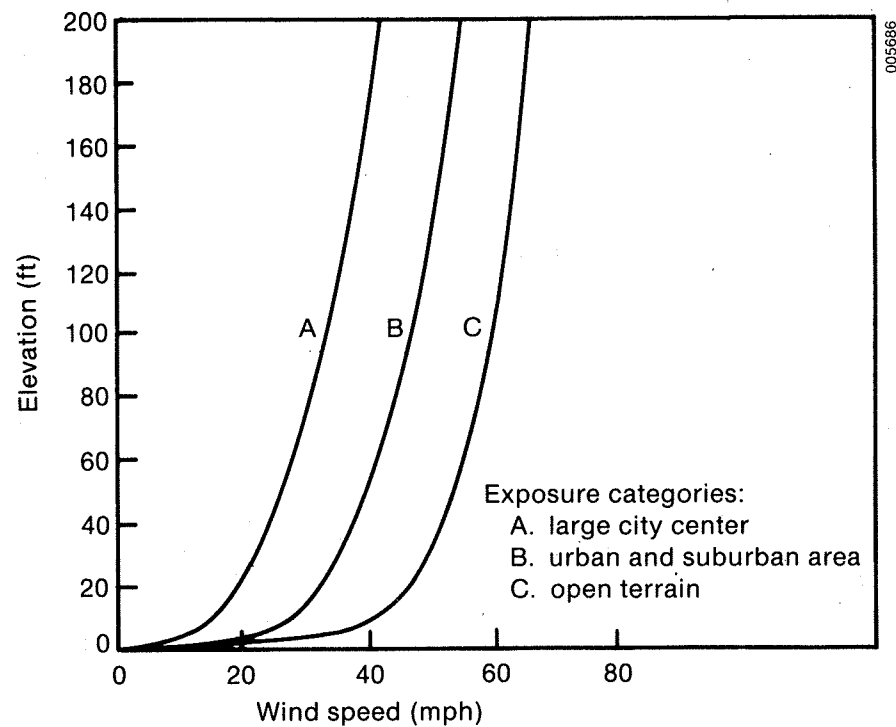


Figure 2-3. Variation of Wind Speed with Elevation, $(U_{30})_C = 50$ mph

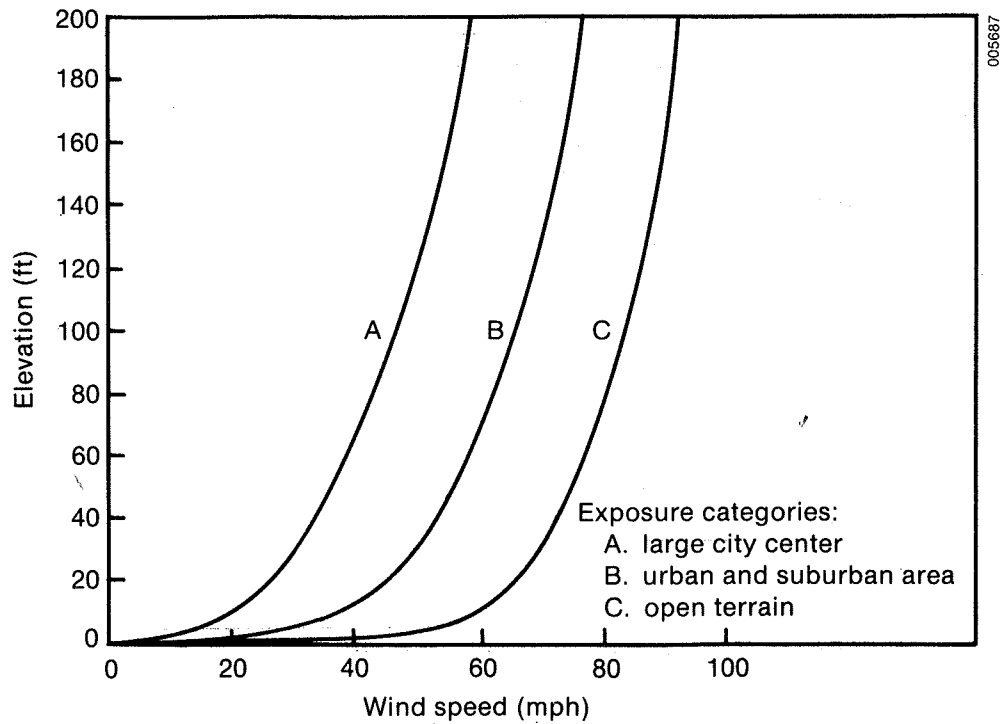


Figure 2-4. Variation of Wind Speed with Elevation, $(U_{30})_C = 70$ mph

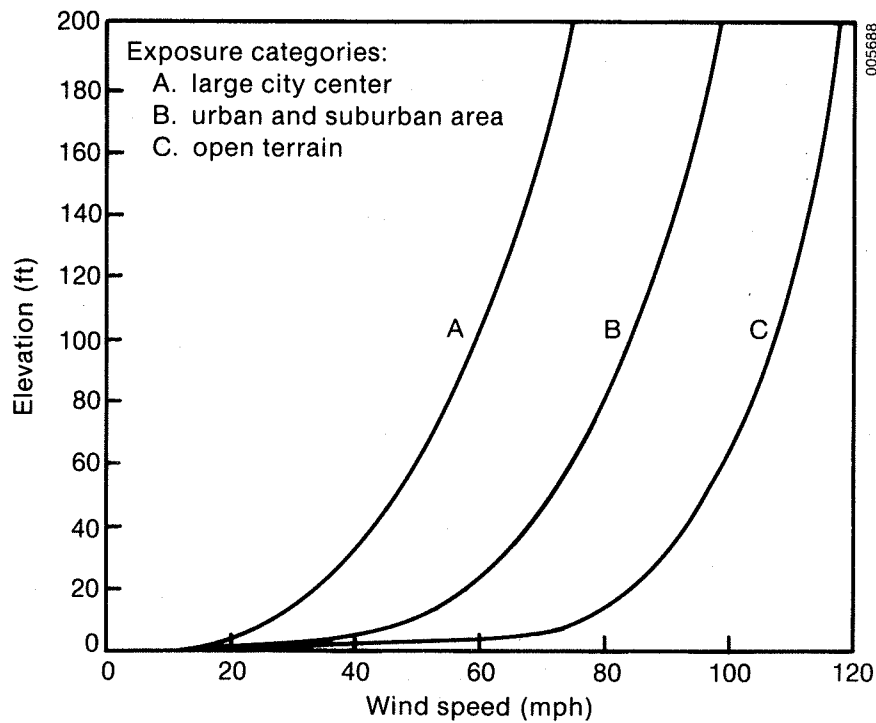


Figure 2-5. Variation of Wind Speed with Elevation, $(U_{30})_C = 90$ mph

Table 2-6. Velocity Pressure

Wind Velocity V (mph) ^a	Dynamic Pressure $q = 0.00256 V^2$ (lb/ft ²) ^b	Wind Velocity V (mph)	Dynamic Pressure $q = 0.00256 V^2$ (lb/ft ²)
10	0.26	220	124
20	1.0	240	147
30	2.5	260	173
40	4.1	280	201
50	6.4	300	230
60	9.2		
70	12.6		
80	16.4		
90	20.7		
100	25.6		
120	37.0		
140	50.2		
160	65.5		
180	83.0		
200	102.4		

^aTo convert to m/s, multiply by 0.447.

^bTo convert to Pa, multiply by 47.88.

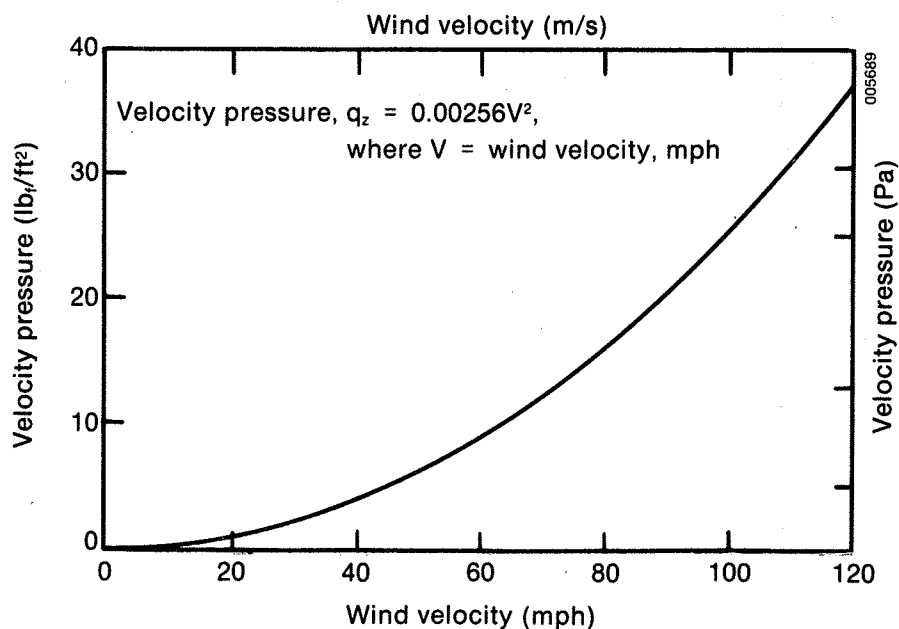


Figure 2-6. Variation of Velocity Pressure with Wind Velocity

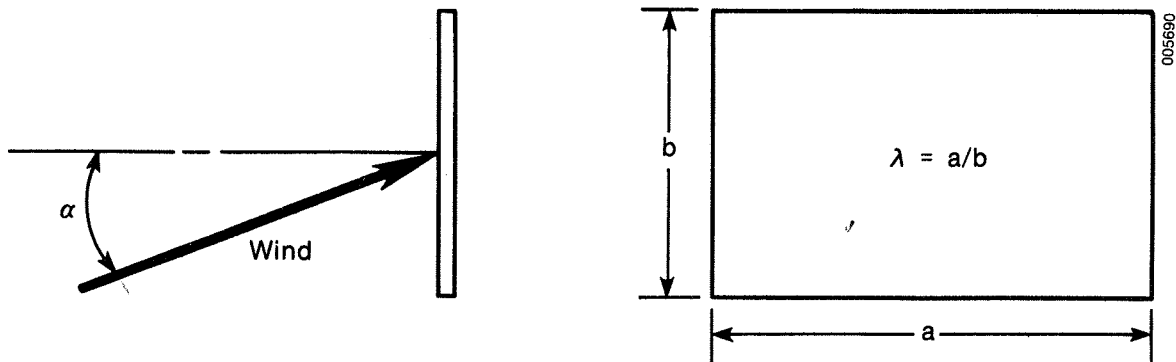


Figure 2-7. A Geometry for Flow past a Flat Plate

Table 2-7. C_f for Flow past a Flat Plate,^a
Aspect Ratio, $\lambda = 1.0$

Angle of Attack α (deg)	C_f (Code)	C_f Task Comm.	$\frac{C_{f_{code}}}{C_{f_{TC}}}$	C_f HelioStat Full-Scale Test ^b	$\frac{C_{f_{code}}}{C_{f_{helioStat}}}$
0	0	0	0	0	0
10	0.45	0.39	1.15	0.39	1.15
15	0.70	0.62	1.13	0.64	1.09
20	0.90	0.84	1.07	0.84	1.07
25	1.15	0.96	1.20	0.98	1.17
30	1.30	1.04	1.25	1.07	1.21

^aCode values are given only up to $\alpha = 30^\circ$.

^bSee Peglow [16].

Table 2-8. C_f for Flow past a Flat Plate,
Aspect Ratio, $\lambda = 3.0$

Angle of Attack α (deg)	C_f (Code)	C_f Task Comm.	$\frac{C_{f_{code}}}{C_{f_{TC}}}$
0	0	0	0
10	0.70	0.57	1.23
15	0.90	0.72	1.25
20	0.95	0.78	1.22
25	1.05	0.84	1.25
30	1.10	0.88	1.25

An important feature of the ANSI code is that the minimum angle of attack is 10° . The code does not consider any angle of attack less than 10° .

The selection of the angle of attack, particularly in the stowed horizontal position of the heliostat, must be made with careful consideration of the meteorological and turbulence characteristics of the high speed air flow. Normally the air flows horizontally over the surface of the earth with a relatively small vertical component. The vertical component arises from two basic sources: surface roughness and instabilities in the air caused by temperature, density, and moisture differences. The first source is essentially mechanical and the second is thermodynamic. In the present study, our primary concern is mainly for the situation when survival requirements (90-mph winds) dictate that the heliostats be placed in the horizontal stow position. Such

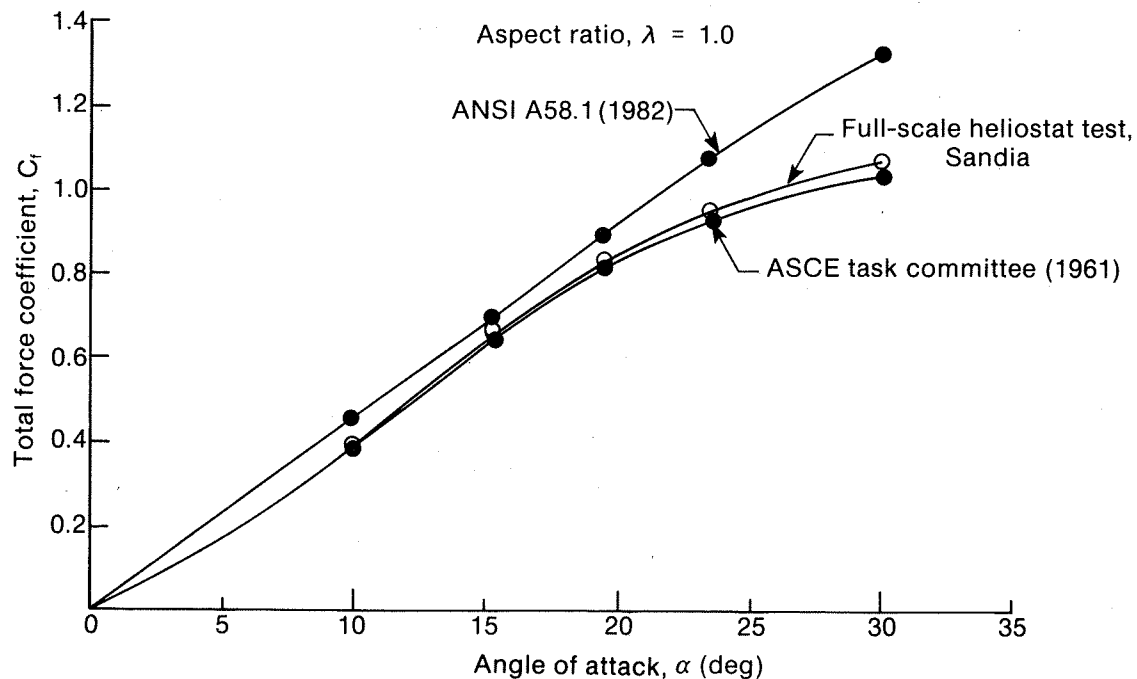


Figure 2-8. Variation of Force Coefficient with Angle of Attack,
Aspect Ratio, $\lambda = 1.0$

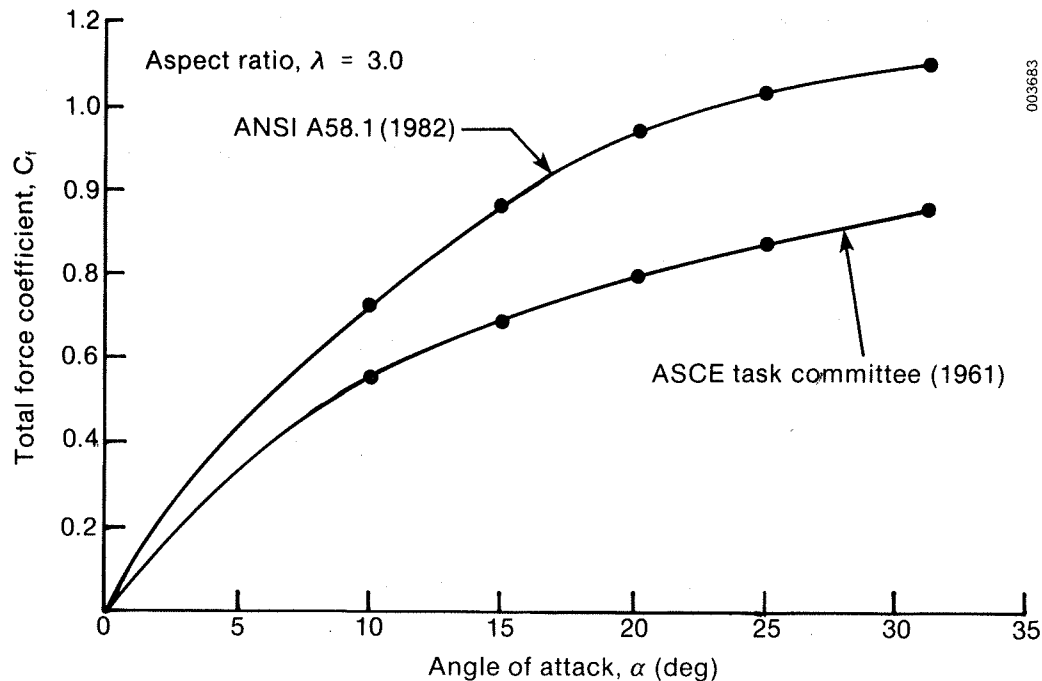


Figure 2-9. Variation of Force Coefficient with Angle of Attack, Aspect Ratio, $\lambda = 3.0$

high wind generally occurs during neutral atmospheric stability, and there is little vertical movement of air caused by thermodynamic effects. It appears that the dominant causes of the vertical component of air velocity are turbulence effects. The force of turbulence-induced vertical fluctuating air acting on the horizontal heliostat can be estimated from the knowledge of the turbulent energy spectra of the approach wind.

2.1 ATMOSPHERIC TURBULENCE SPECTRA

The random fluctuations of velocity in a turbulent flow passing a point in the flow field may be caused by the superposition of the local vortices or eddies, each with a random motion of frequency n (alternatively of wave number k). We can approximate the total kinetic energy of the turbulent motion by summing the contributions of each eddy in the flow. When the equations of motion of turbulent flow are appropriately transformed and analyzed, it can be shown that the inertial transfer of energy from the larger eddies to the smaller eddies takes place; the viscous dissipation takes place primarily in the smallest eddies through shear deformations. The cascade process of kinetic energy transfer from the larger eddies to the smaller ones, and ultimately energy dissipation into heat, is the basic postulate of Kolmogorov's hypothesis.

Measurements of turbulent spectra in the surface layer of the atmosphere substantiate the validity of the assumptions regarding the turbulent energy transfer mechanism. In an idealized horizontally homogeneous, neutrally stable flow, the energy production rate is approximately balanced by the energy dissipation rate.

The wind velocity varies randomly with time. As a result, the wind pressures on the surface of the structure are not steady; they also vary with time. The mean square dynamic pressure is related to the mean square longitudinal velocity fluctuations, which implies that the pressure spectrum is proportional to the spectrum of the longitudinal velocity. The spectrum of dynamic pressure can be predicted from the known longitudinal velocity spectrum.

The estimation of "gust response factor" used to determine the wind force on the structure is based on the design methodology developed by Vellozzi and Cohen [6]. The methodology uses the results of the power spectrum analysis of the dynamic structural response of simple linear single one degree of freedom system with viscous damping and measured wind gust spectra and gust correlation coefficient. The various turbulent wind spectra, commonly used in the study of lower atmosphere, are compared to assess the energy spectra used in the ANSI building code.

The spectrum $S(z,n)$ of the longitudinal velocity fluctuations in the inertial subrange can be expressed in the following normalized form [24]:

$$\frac{n S(z,n)}{U_*^2} = 0.26 f^{-2/3}, \quad (2-15)$$

where

$$f = \frac{n z}{U(z)}, \quad n = \text{frequency}$$

$$U_* = \text{friction velocity}$$

$$z = \text{elevation}$$

$$U(z) = \text{mean velocity at height } z.$$

The left-hand member of Eq. 2-15 is called the reduced spectrum of the longitudinal velocity fluctuations and is a function of height. Simiu [25] considers Eq. 2-15 a good representation of spectra in the high-frequency range and suggests using it for $f > 0.2$.

The longitudinal energy spectra currently employed in the ANSI A58.1-1982 building code can be expressed by the following empirical relation [25]:

$$\frac{n S(z,n)}{U_*^2} = \frac{4x^2}{(1 + x^2)^{4/3}}, \quad (2-16)$$

where

$$x = \frac{1200n}{U(10)}$$

$$U(10) = \text{mean wind speed at height 10 m (mph, m/s)}.$$

Equation 2-16 was obtained by averaging the results of the measurements at various heights and does not, therefore, show the dependence of spectra on height.

In the low-frequency range the energy spectra cannot be described by a universal relation. Kaimal et al. [26] considered the limiting value of the spectra as f approaches zero, and the product $n S(z,n)$ reaches a maximum value at $f = f_m$ such that $0 < f_m < f_S$. Equation 2-15 is valid beyond the value of $f = f_S$. Kaimal et al. [26] proposed the following empirical relation for the longitudinal spectra in the low frequency range:

$$\frac{n S(z,n)}{U_*^2} = \frac{200f}{(1 + 50f)^{5/3}} \quad (2-17)$$

Equation 2-17 approximates closely the spectrum in the higher frequency range also, and Simiu [25] suggested using it for the entire spectrum.

The spectra that Lumly and Ponofsky [27] developed for the vertical and lateral velocity fluctuations in the lower surface layer of the atmosphere are given, respectively, by the empirical relations:

$$\frac{n S_w(z,n)}{U_*^2} = \frac{3.36f}{(1 + 10f)^{5/3}} \quad (2-18)$$

and

$$\frac{n S_v(n)}{U_*^2} = \frac{15f}{(1 + 9.5f)^{5/3}} \quad (2-19)$$

Equation 2-16 was obtained by averaging results of measurements obtained at various heights above the ground and does not reflect the dependence of spectra on height. However, the dependence of spectra on height is clearly suggested by Davenport [28]. The spectral distribution in the lower frequency range has little influence on the structural response. However, the magnitude of the turbulent fluctuation components at the natural frequencies of the structure (or of one or more of its major elements) may affect its response significantly. Simiu [25] considered a wind velocity of 30 m/s and a surface roughness $z_0 = 0.08$ m and computed the longitudinal spectra in the frequency range of 0.001-0.5 Hz by using Eqs. 2-16 and 2-17. He considered heights $z = 100.0$ m, 200.0 m, and 300.0 m. The comparison showed that the expression currently used in building codes overestimated the longitudinal spectra of turbulence in the higher frequency range by as much as 100%-400%.

To compare the spectra obtained using Eqs. 2-15 through 2-19, computations were made for two wind velocities, namely $U(z) = 44.73$ mph and $U(z) = 90.0$ mph at a height of $z = 30.0$ ft. This height was chosen to conform to the requirement of the ANSI code. Figure 2-10 shows the longitudinal spectra computed by Eqs. 2-15, 2-16, and 2-17 for wind velocity $U = 44.73$ mph (20.0 m/s). The building code spectra overestimate the Kaimal spectra in the frequency range of 0.007-0.08 Hz and underestimate beyond the frequency $n = 0.08$ Hz. Figure 2-11 shows the longitudinal, lateral, and vertical spectra of turbulence of 44.73-mph wind at a height of 30.0 ft. At frequency $n = 1.0$ Hz, the local isotropy is realized. For frequency less than 1.0 Hz, the vertical spectral energy content is less than these for the longitudinal and lateral components. Figure 2-12 shows the energy spectra of turbulence for a 90.0-mph wind at an elevation of 30.0 ft.

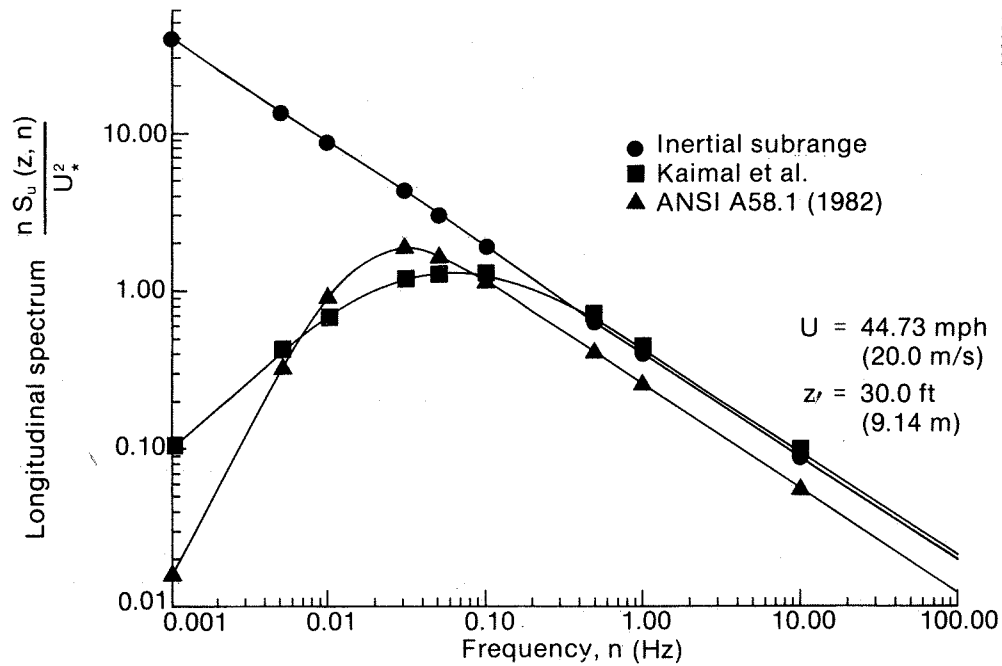


Figure 2-10. Longitudinal Turbulence Spectra,
 $U = 44.73$ mph (20.0 m/s)

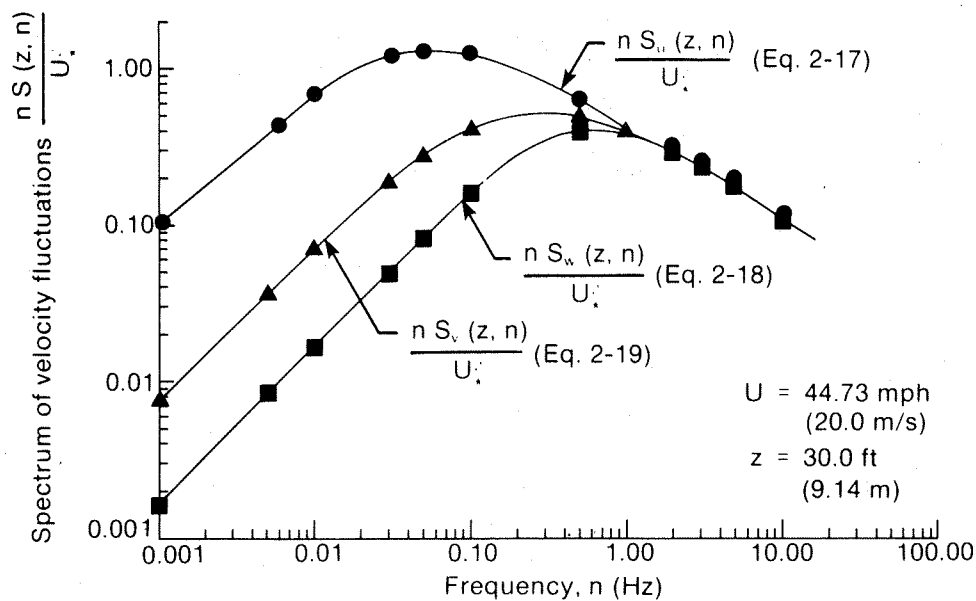


Figure 2-11. Turbulent Wind Spectra,
 $U = 44.73$ mph (20.0 m/s)

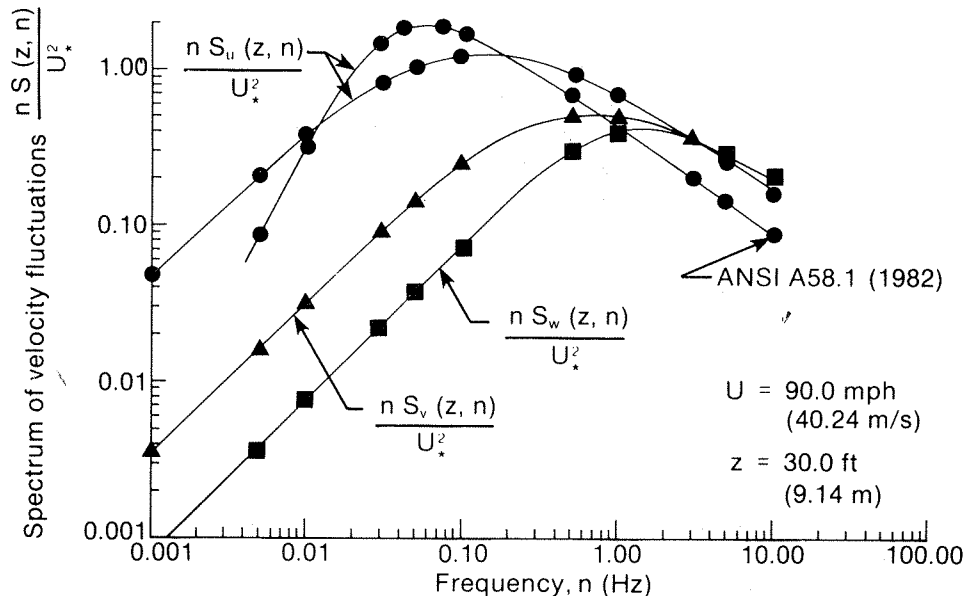


Figure 2-12. Turbulent Wind Spectra,
 $U = 90.0$ mph (40.24 m/s)

2.2 VARIATION IN WIND ANGLE FROM THE HORIZONTAL

The vertical wind components fluctuate randomly at various rates. When the heliostats are stowed in a horizontal position, the effect of the longitudinal component of the wind velocity on the heliostats is relatively small. However, the peak angle of attack of the vertical turbulent component of wind velocity may have a significant effect on the structure. The angle of attack stipulated in the ANSI code is rather large. According to the code, the minimum angle of attack on a flat plate must be 10° .

The methodology developed by Daniels [29] is used to estimate the probable value of the peak angle of attack on the heliostat in the horizontal position. According to Daniels, the lateral spectra are the basis for determining the lateral angle of attack. Since the vertical spectral energy content is generally less than that of the lateral spectra, Daniels suggests that the angle of attack will give correct values at frequencies beyond $n = 3.0$ Hz if it is determined on the basis of the lateral spectra. The angle of attack will be somewhat overestimated for values of frequency less than $n = 3.0$ Hz. Accordingly, the angles of attack for wind velocities of 30.0, 50.0, and 90.0 mph at an elevation of 30.0 ft are estimated. First, we determine the angle of attack for the lateral component of turbulent velocity. Then, by comparing the magnitude of the lateral and vertical spectra at their peak frequencies, we use a correction factor to estimate the angle of attack for the vertical component of the turbulent velocity.

The along-wind spectra are represented by the curve marked "longitudinal," and across-wind spectra are represented by the curve marked "lateral." The longitudinal and lateral spectral values $S(\omega)$ at a frequency ω and height z are given in the form of a dimensionless formula:

$$\frac{\omega S(\omega)}{\beta U_*^2} = \frac{c_1 f/f_m}{\{[1 + 1.5 (f/f_m)c_2]^{5/3}\}c_2}, \quad (2-20)$$

where

$$f = \frac{\omega z}{U(z)},$$

$$f_m = c_3 (z/z_r)^{c_4},$$

$$\beta = \left(\frac{z}{z_r}\right)^{c_5},$$

and

$$U_* = \frac{0.4 U(z)}{\ln \frac{z_r}{z_0} - \Psi}.$$

Daniels' velocity spectra for strong wind conditions are shown in Figure 2-13.

In the above equations z_r is the reference height equal to 60 ft (18.3 m) for the sites and the values of the constants suggested (shown in Table 2-9); z_0

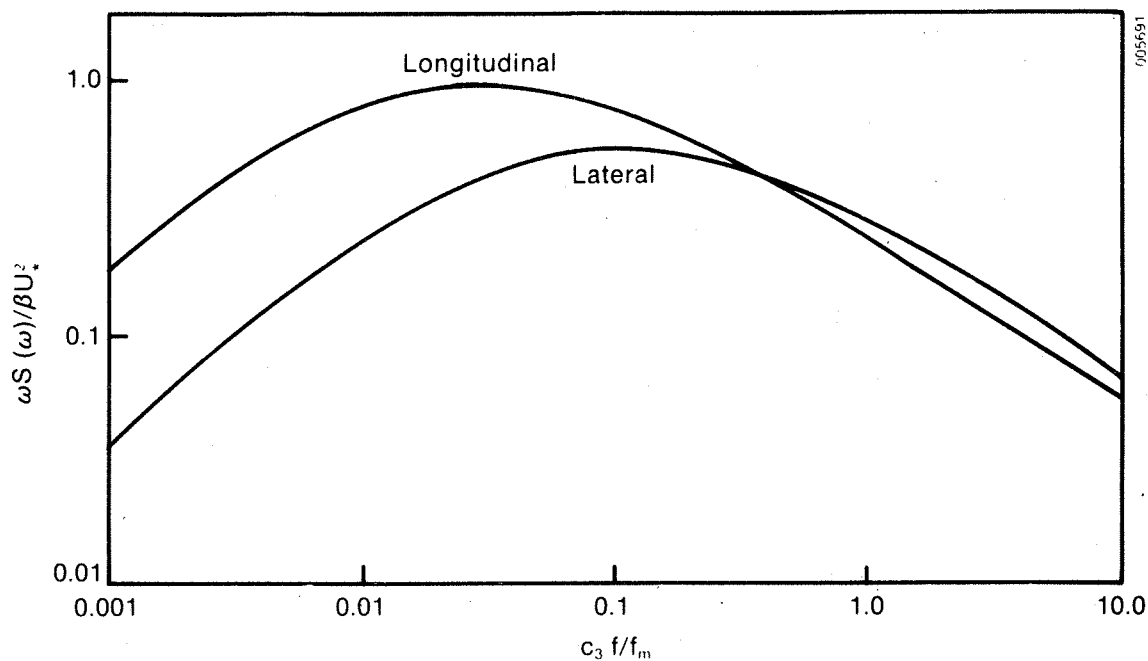


Figure 2-13. Strong Wind Velocity Spectra
Source: Ref. 29.

Table 2-9. Dimensionless Constants for Longitudinal and Lateral Turbulence Spectra

Condition	Constant				
	c_1	c_2	c_3	c_4	c_5
Strong wind (Longitudinal)	6.198	0.845	0.03	1.00	-0.63
Strong wind (Lateral)	3.954	0.781	0.10	0.58	-0.35

Source: Ref. 29.

is the surface roughness at the site; Ψ is a stability parameter depending on the atmospheric stability; $U(z)$ is the mean longitudinal wind speed at a height z ; and c_1 , c_2 , c_3 , c_4 , and c_5 are dimensionless site-specific constants. The parameters β and f_m account for height effects and are used in normalizing the dimensionless quantities

$$\frac{\omega S(\omega)}{\beta U_*^2} \quad \text{and} \quad \frac{c_3 f}{f_m} .$$

The following parameters are required to estimate the angle of attack for the lateral component of the turbulent fluctuating velocity: the elevation Z , the mean longitudinal wind speed $U(z)$ at that height, and the characteristic roughness length z_0 of the site. Using the relations given in Eq. 2-20, the values of the parameters β , U_* , and f_m are computed. To estimate the amplitude of the lateral component of turbulent velocity v_0 , a simple sinusoidal model is used. It can be assumed that

$$v(t) = v_0 \sin 2\pi\omega t , \quad (2-21)$$

where

v_0 = amplitude of lateral velocity

ω = frequency in Hz

t = time (s).

The frequencies ω for low-frequency spectrum analysis are in the range of 0.01-1.0 Hz. The peak frequency is approximately $\omega = 0.1$ Hz and is used to calculate the normalized frequency f . The normalized frequency parameter $0.1 f/f_m$ on the abscissa of Figure 2-13 is then computed, and Figure 2-13 is used to get the value of $\frac{\omega S(\omega)}{\beta U_*^2}$ from the ordinate. For strong wind conditions, the stability parameter vanishes and is neglected in evaluating the friction of velocity U_* .

It can be shown [18] that at a particular frequency ω ,

$$\omega S(\omega) = \int_0^{2\pi} [v(t)]^2 dt . \quad (2-22)$$

Using the relation of $v(t)$ from Eq. 2-21, Eq. 2-22 can be reduced to

$$\omega S(\omega) = \frac{v_o^2}{2} . \quad (2-23)$$

Equation 2-23 is used to estimate the magnitude of peak lateral velocity:

$$v_o = [2\omega S(\omega)]^{1/2} . \quad (2-24)$$

The angle of attack α_v for lateral fluctuating velocity is obtained from the following relationship:

$$\alpha_v = \tan^{-1} \left| \frac{v_o}{U(z)} \right| . \quad (2-25)$$

Since the magnitude of lateral spectra is approximately 1.21 times larger than that of the vertical spectra, the amplitude of vertical fluctuating velocity w_o is approximately equal to $0.91v_o$. The angle of attack for the vertical component of fluctuation is given by

$$\alpha_w = \tan^{-1} \left(\frac{0.91v_o}{U(z)} \right) . \quad (2-26)$$

The angles of attack for lateral and vertical components of fluctuating velocities have been computed for each of three mean longitudinal velocities of 30.0, 50.0, and 90.0 mph at the standard elevation of 30.0 ft for various surface roughness lengths. The results are tabulated in Tables 2-10 and 2-11, and shown graphically in Figures 2-14 and 2-15. When the surface roughness length z_o of a site is small, the values of the angle of attack are relatively less. The values increase as the roughness length increases. One interesting feature of the present analysis is that when the mean wind speed increases, the values of the angle of attack decrease. The design angle of attack

Table 2-10. Variation of Angle of Attack due to Fluctuating Lateral Velocity

Roughness Height, z_o	Angle of Attack, α (deg)		
	$U(30) = 30.0$ mph	$U(30) = 50.0$ mph	$U(30) = 90.0$ mph
0.10 ft (0.031 m)	4.53	4.44	4.15
0.20 ft (0.061 m)	4.039	3.96	3.70
0.40 ft (0.123 m)	5.14	5.05	4.72
1.312 ft (0.4 m)	6.73	6.61	6.19
1.968 ft (0.60 m)	7.52	7.37	6.90
2.624 ft (0.80 m)	--	--	7.53

Table 2-11. Variation of Angle of Attack due to Fluctuating Vertical Velocity

Roughness Height, z_0	Angle of Attack, α_w (deg)		
	$U(30) = 30.0$ mph	$U(30) = 50.0$ mph	$U(30) = 90.0$ mph
0.10 ft (0.031 m)	3.68	3.60	3.37
0.20 ft (0.062 m)	4.12	4.04	3.78
0.40 ft (0.123 m)	4.68	4.60	4.30
1.312 ft (0.40 m)	6.13	6.02	5.64
1.968 ft (0.60 m)	6.85	6.71	6.28
2.624 ft (0.80 m)	--	--	6.86

suggested by the ANSI A58.1-1982 code is 10° . The recent improved value of the angle of attack suggested by Murphy [14] is 6° .

The McDonnell Douglas Astronautics Company (MDAC) [30] reported that a maximum of a 6.5° angle of attack could be expected for high winds in gentle, rolling terrain with a roughness length of 4.0 cm.

Vann [31] used Daniel's approach and estimated the angle of attack due to lateral fluctuations for wind velocity $U = 30.0$ mph (13.41 m/s), at height $z = 30$ ft, for surface roughness $z_0 = 3.0$ ft. He considered the lateral spectra as representative of vertical spectra. The estimated peak angle of attack

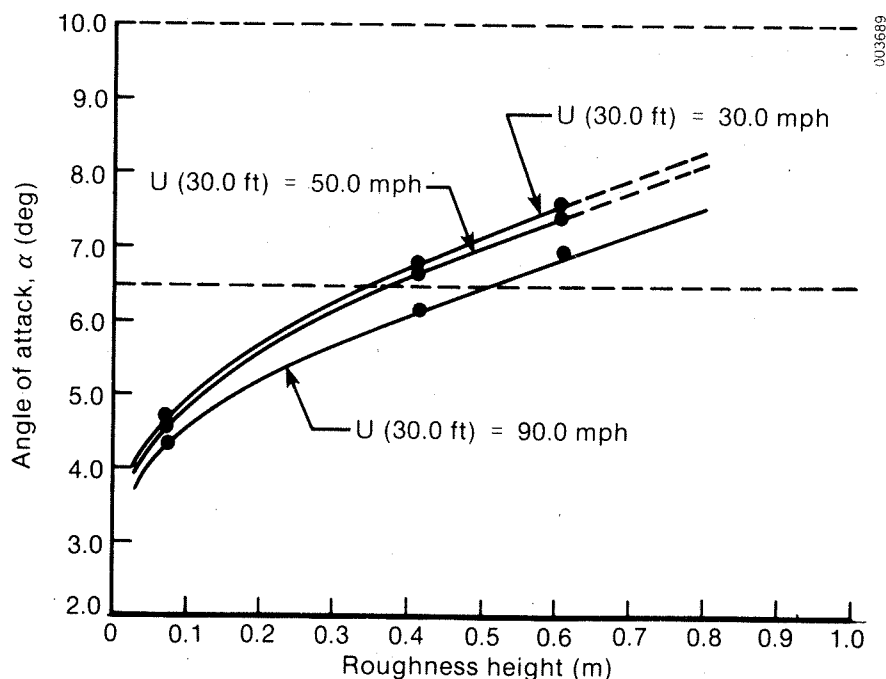


Figure 2-14. Peak Angle of Attack due to Turbulent Lateral Velocity

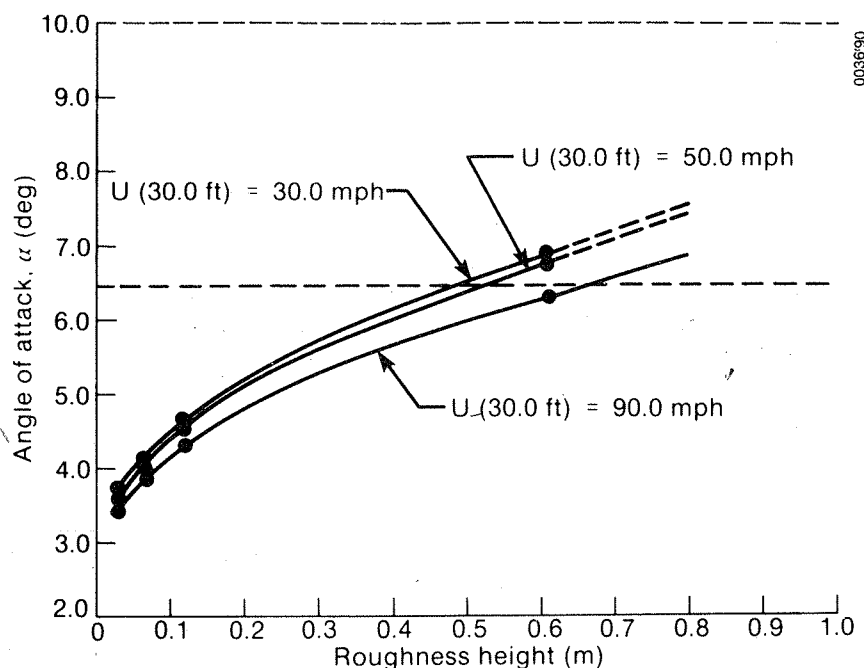


Figure 2-15. Peak Angle of Attack due to Turbulent Vertical Velocity

at $\omega = 0.1$ Hz was 8.9° . The surface roughness z_0 of 3.0 ft (0.91 m) is rather too large. The surface roughness value is a significant parameter in the determination of the peak angle of attack due to turbulent velocities. The values of the peak angle of attack increase as the surface roughness increases. One interesting feature of the present analysis is that the value of the angle of attack decreases with the increase of the mean wind speed. Figure 2-15 shows that for $0.2 \text{ m} < z_0 < 0.4 \text{ m}$ the estimated peak angle of attack due to turbulent vertical velocity for a 90-mph wind and heliostat stored in horizontal position is in the range of 4.8° – 5.6° . Estimating the peak angle of attack is quite involved. To obtain more reliable values for the angle of attack, recourse should be taken to either full-scale field study or model study in a simulated flow field in the environmental wind tunnel.

Simiu and Scanlan [25, Table 2.2.1] give typical values of surface roughness z_0 for various types of surfaces and corresponding values of the surface drag coefficients. The table also includes the suggested values of z_0 for built-up terrains such as outskirts of towns and suburbs, centers of towns, centers of large cities, etc. The suggested value of z_0 for outskirts of towns and suburbs is in the range of 0.20–0.40 m; for the open fields, z_0 is in the range of 0.01–0.1 m depending on the physical characteristics. Figure 2-15 shows that for $0.2 \text{ m} < z_0 < 0.4 \text{ m}$, the estimated angle of attack for a 90-mph wind and heliostat stowed in a horizontal position is in the range of 4.8° – 5.6° . If the lower z_0 values are used for the heliostat field, the values of the angle of attack are smaller. Figure 2-14 and Figure 2-15 show clearly that the ANSI code values for the angle of attack are too high.

SECTION 3.0

REDUCTION OF WIND LOADING

Recent studies [14,15,16,21,22,32] of scale models of solar collectors in environmental wind tunnels show that the present method of determining wind loads on solar collectors, photovoltaic arrays, and heliostats using the guidelines outlined in the ANSI A58.1-1982 building code requirements for minimum design loads in buildings and other structures [12] is conservative. Much of the available information indicates that the degree of conservatism is significant, but the actual extent of that conservatism must be assessed in more detail. The code was not developed for the low-height structures like solar collectors. The pertinent site-specific meteorological data such as wind velocity distribution in the lower atmosphere, stability features, and turbulent characteristics of the wind field are not reliably known. Since the wind profile changes [25] with the changes of the roughness length z_0 of the locality of the structure, values depending solely on the airport data should not be used in optimum design without carefully considering the terrain conditions, local surface roughness, orientation of the heliostats, and direction of the wind.

Ravindra et al. [33] developed an interesting methodology to determine the design wind loads on structures based on the statistical parameters of the lifetime maximum wind speed, the annual maximum wind speed, and the daily maximum wind speed. Ravindra et al. use the general equation for determining the wind pressure and consider all the parameters (pressure coefficient, effective velocity pressure, velocity pressure coefficient that depends on the type of exposure and height above the ground, gust factors that depend on the response characteristics of the structure, and the basic wind speed measured at the reference height) as random variables. The mean wind pressure and coefficient of variation of the wind pressure are expressed as functions of the mean and the coefficient of variation of the random variables. Laboratory test results are used to obtain values of coefficients of variation.

Generally, the statistics of wind directions are not considered in the code. Davenport [34] considered two cases of loadings: (1) the direction of maximum wind is uniformly distributed between $+\pi$ and $-\pi$, corresponding to the assumption that the worst response occurs no matter what the wind direction is; and (2) the direction of maximum wind is distributed according to a cosine law. The ratio of the mode in case 2 to the mode value in case 1, called the direction reduction factor, has been estimated to be 0.72. Ravindra et al. [33] considered other factors, such as serviceability and ultimate limit state, and recommend that the mean design wind pressure be reduced by a design resistance factor of 0.75. Reducing the wind load by 25% for the variability of wind direction and other considerations should be viewed with caution. Results from simulated laboratory or field studies should be used to estimate the reduction of wind loads caused by the variation in wind direction.

Modification of the shear layer that develops over the heliostat surface is an area of study that may lead to the reduction of drag experienced by the heliostats. Melbourne [35] and Gartshore [36] observed that the small-scale

turbulence increases significantly in the reattaching shear layers on the surface and consequently increases the magnitude of the high negative surface pressure. It is reasonable to consider that venting the region of separated flow and its subsequent reattachment may be useful in reducing the magnitude of negative pressure. Melbourne [35] observed that venting the separated flow region reduced the negative pressure thereby leading to increased flow stability. It is well known that a pressure reduction (below ambient) on the streamwise surfaces near the leading edge of the flat plate occurs in the region of flow separation. Venting or introducing fluid with a higher level of momentum in the region (the bubble under the reattaching shear layer) is an old technique to delay flow separation and decrease the reduced pressure effect. This can be accomplished by using a slotted eave along the periphery of the surface.

The heliostat modules have sharp edges, and under regular and horizontal stow positions, flow separations near the leading edge and subsequent reattachment occur. A porous eave around the edges of the scale model of a module would be useful for testing in an environmental wind tunnel under simulated flow conditions. Streamlining the windward and leeward edges may be helpful in reducing and even eliminating flow separation and subsequent reattachment.

The air gap between the modules allows high-momentum air to flow through the array and is expected to reduce the windward pressure as well as the negative pressure on the back side. The appropriate amount of air gap for total drag reduction needs to be determined from laboratory tests in the simulated flows. Investigations of the effects of high porosity in a flat plate on the reduction of total drag may lead to basic knowledge of drag control by allowing high-momentum fluid in the wakes of a flat plate. The test results of Xerikos et al. [17] did not show significant drag reduction because the slot openings were rather small. A preliminary study of the effects of the solidity ratio of a flat plate placed normal to the flow in the boundary layer by Rangwala and Handy [37] showed that considerable reduction in drag is possible when the solidity ratio is less than 70%.

Experimental results from the wind tunnel study [17] indicated that placing heliostats in the wakes of the heliostats in front helped to reduce wind loads on the heliostats in the wakes. However, wind directions, turbulent intensity, and dynamic response of the structure due to increased turbulence in the wake regions may influence the net outcome. In the simulated flow fields in the wind tunnel, we need to study the development of wakes behind the heliostats in the inner part of the field to gain knowledge of the relative magnitude of the force and moment coefficients that are needed to adequately estimate the wind load on a heliostat.

Perimeter fences [38] are effective in reducing wind loads on the photovoltaic arrays. Fence porosity of 30%-50% and fence height approximately equal to three-quarters of the array height enhance the reduction of wind loads significantly. However, the effect is only limited to the first few rows of arrays along the perimeter. Fences inside the heliostat field, placed at experimentally determined strategic positions, may be helpful to reduce the base-bending moment of the heliostat.

The experimental works of Randall et al. [39,40] with parabolic trough solar collectors are of great practical importance. The significant interference effect provided by the upstream collector rows on the lateral and lift forces indicates that most collector modules within an array experience force reduction. Randall et al. have studied the influence of the height of a fence placed three aperture widths upstream of the first row of collectors. The test results indicate that a fence height somewhat less than the full collector height provides the major part of the force reduction. Similar results are also obtained for the influence of the berm height.

Shelter belts made up of trees, shrubs, and other small structures acting as wind breakers along the perimeter of the heliostat field may be helpful in reducing the effective wind velocity in the field. Sturrock [41] observed that properly designed shelter belts and wind barriers could be significantly effective in reducing wind load on structures. It is possible to study and evaluate the effectiveness of the barrier in the wind tunnel.

The packing density [42] of heliostats in the field had discernible effect on the resulting wind loads. Higher packing density will reduce net wind load on the heliostats. It might be feasible to develop an optimum design of the heliostat field with relatively higher density in the outer part of the field.

The heliostats at the outer periphery of the field are subjected to maximum wind load; therefore, they should be designed structurally stronger and more rigid. It is possible to use less rigid and relatively lighter support structure for the heliostats in the interior of the field.

SECTION 4.0

CONCLUSION AND RECOMMENDATIONS

This study was limited to reviewing and assessing the present design methodology for wind loading on solar collectors, particularly for heliostats, and recommending areas of further investigation to develop realistic criteria for determining adequate wind loads. The results and conclusions of the study can be summarized as follows:

- The present methodology for designing wind load using the outlines given by the ANSI A58.1-1982 Code is conservative.
- The history of the site-specific velocity data is necessary to apply extreme value order statistics for determining design wind speed. Local climatological data including wind directions and surface roughness should be used to develop the velocity profile.
- Comparative study of the total force coefficient of a flat plate of various aspect ratios and at various angles of attack shows that the values obtained by using the ANSI Code are always higher.
- The energy spectra obtained by the formulas suggested by various authorities were compared with the energy spectra for the code and show that in the flow-frequency domain, the code overestimates spectral values for lower frequencies but underestimates in the region of higher frequencies, including the natural frequencies of heliostats and other solar collectors.
- The angle of attack that results from the fluctuating vertical wind is considerably smaller than the value suggested by the code.
- Development of locally modified flow over the heliostat has the potential to reduce wind load on the heliostat.
- Appropriate ventilation in the heliostat modules has the potential to reduce dynamic wind load.

Recommendations for further studies that might reduce wind loading on the collector are stated briefly:

- Modifying the flow locally by using a turbulence stimulator in the form of porous eaves around the heliostat will discourage the flow separation at the edges of the heliostats and help to reduce dynamic wind load.
- Investigating the effect of appropriate gaps between the modules will encourage ventilation around the module.
- Studying the effects of the perimeter fences and fences in the field around a group of heliostat zones will be useful in overall wind-load reduction.
- Developing a wind rose for the heliostat field to estimate the statistics of variation of wind direction. The terrain and topographical aspects of the heliostat field play important local roles in determining the magnitudes of wind speed and direction. The wind direction is not considered

in the building code. The statistics of the directional variability of the wind are essential in determining wind load reliably.

SECTION 5.0

REFERENCES

1. Pugsley, A., "The Safety of Structures," Baltimore, MD: Edward Arnold, 1966.
2. Davenport, A. G., "Estimation of Repeated Loads on Structures with Application to Wind Induced Fatigue and Overload," Proceedings of RILEM International Symposium: Effects of Repeated Loading of Materials and Structures, Vol. 38, 1967.
3. Robertson, L. E., "On Tall Buildings," Proceedings of a Symposium on Tall Buildings, University of Southampton, edited by A. Coull and B. Stafford-Smith, Oxford, U.K.: Pergamon Press, 1967.
4. Davenport, A. G., "The Dependence of Wind Loads on Meteorological Parameters," Proceedings of International Research Seminar on Wind Effects on Buildings and Structures, Ottawa: National Research Council of Canada, 1967.
5. Davenport, A. G., "The Nature of Disturbing Forces," Proceedings of RILEM International Symposium: Effects of Repeated Loading of Materials and Structures, Mexico, 1966.
6. Vellozzi, J., and E. Cohen, "Gust Response Factors," Journal of the Structural Division, American Society of Civil Engineers, Vol. 94, ST 6, June 1968.
7. Davenport, A. G., "A Rationale for Determination of Design Wind Velocities," J. Structural Division, American Society of Civil Engineers, Vol. 86, No. ST 5, Proc. Paper 2476, May 1960.
8. Gumbel, E. J., "Statistical Theory of Extreme Values and Some Practical Applications," Applied Mathematics Series No. 33, Washington, DC: National Bureau of Standards, 1954.
9. Thom, H. C. S., "Frequency of Maximum Wind Speeds," Proc. Separate No. 539, American Society of Civil Engineers, Vol. 80, November 1954.
10. Lieblein, J., "Method of Analyzing Extreme Value Data," Technical Note 3053, Washington, DC: National Advisory Committee for Aeronautics, 1954.
11. Thom, H. C. S., "New Distribution of Extreme Winds in the United States," J. American Society of Civil Engineers, Vol. 94, No. ST 7, July 1968.
12. American National Standard A58.1-Building Code Requirements for Minimum Design Loads in Buildings and Other Structures, NY: American National Standard Institute, 1982.
13. Simiu, E., "Wind Climate and Failure Risks," J. Structural Division, American Society of Civil Engineers, Vol. 102, ST 9, September 1976.

14. Murphy, L. M., An Assessment of Existing Studies of Wind Loading on Solar Collectors, SERI/TR-632-812, Golden, CO: Solar Energy Research Institute, February 1981.
15. Roschke, E. J., Wind Loading on Solar Concentrators: Some General Considerations, DOE/JPL-1060-66, JPL Publication 83-101, Pasadena, CA: Jet Propulsion Laboratory, May 1984.
16. Peglow, S. G., Wind Tunnel Test of a Full Scale Heliostat, SAND 79-8034, Livermore, CA: Sandia Laboratories, June 1979.
17. Xerikos, J. et al., "The Aerodynamics of Heliostats for Solar Power Plant Applications," Proceedings of the 5th International Conference on Wind Engineers, 1979, 2 vols., edited by J. E. Cermak, Oxford, U.K.: Pergamon Press, 1980.
18. McDonald, J. R., Wind Effects on Solar Tower Generator, Lubbock, TX: Institute for Disaster Research, Texas Tech University, 1978.
19. Cermak, J. E., "Applications of Fluid Mechanics to Wind Engineering--A Freeman Scholar Lecture," J. Fluid Engineering, Vol. 97, March 1975.
20. Bhaduri, S., "Simulation of Urban Atmosphere for Diffusion Study," Engineer, Vol. VI, No. 2, 1973.
21. Lindsay, J. E., Force and Pressure Tests of Solar Collector Models in the Vought Corporation Systems Division Low Speed Wind Tunnel, SAND 76-7007, Albuquerque, NM: Sandia Laboratories, May 1979.
22. Randall, D. E., D. D. McBride, and R. E. Tate, Parabolic Trough Solar Collector Wind Loading, SAND 79-8034, Albuquerque, NM: Sandia Laboratories, June 1979.
23. Task Committee on Wind Forces, "Wind Forces on Structures," Transactions, American Society of Civil Engineers, Vol. 126, No. 3269, 1961.
24. Simiu, E., "Wind Spectra and Dynamic along Wind Response," J. Structural Division, American Society of Civil Engineers, Vol. 100, No. ST9, September 1974.
25. Simiu, E., and R. H. Scanlan, Wind Effects on Structures, NY: John Wiley and Sons, 1978.
26. Kaimal, J. C., et al., "Spectral Characteristics of Surface-Layer Turbulence," J. Royal Meteorological Society, Vol. 87, 1961.
27. Lumley, J. L., and H. A. Panofsky, The Structure of Atmospheric Turbulence, NY: John Wiley & Sons, 1964.
28. Davenport, A. G., "The Spectrum of Horizontal Gustiness Near the Ground in High Winds," J. Royal Meteorological Society, Vol. 87, 1961.

29. Daniels, G. E., ed., Terrestrial Environment (Climatic) Criteria Guidelines for Use in Aerospace Vehicle Development, 1973 Revision, NASA TM X-64757, Huntsville, AL: Marshall Space Flight Center, 1973.
30. McDonnell Douglas Astronautics Company, Optimization of the Second Generation Heliostat and Specification, SAND 82-8181, May 1982.
31. Vann, W. P., "Wind Effects on Solar Tower Generators," Final Report, Subcontract No. 77-TT-1 (Sub-Task b.), Lubbock, TX: Energy Foundation of Texas, Texas Tech University, 1978.
32. Bechtel National, Inc., Wind Designs on Flat Panel Photovoltaic Array Structures, SAND 79-7057, Livermore, CA: Sandia Laboratories, 1980.
33. Ravindra, M. K., et al., "Wind and Snow Load Factors for Use in Load and Resistance Factor Design," J. Structural Division, American Society of Civil Engineers, Vol. 104, ST 9, 1978.
34. Davenport, A. G., "The Prediction of Risk under Wind Loading," Proc. of the Second International Conference on Structural Safety and Reliability, Technical University in Munich, Munich, West Germany, Dusseldorf, West Germany: Werner-Verlag, September 1977.
35. Melbourne, W. H., "Turbulence Effects on Maximum Surface Pressures--A Mechanism and Possibility of Load Reduction," Proceedings of the Fifth International Conference on Wind Engineering, Ft. Collins, CO: Colorado State University, July 1979.
36. Gartshore, I. S., "The Effects of Free-Stream Turbulence on Drag of Rectangular Two-Dimensional Prisms," Boundary Layer Wind Tunnel, Report 4-73, Canada: University of Western Ontario, 1973.
37. Rangwala, S., and E. Handy, Drag of a Flat Plate of Variable Solidity Ratio Placed Normal to Flow in a Boundary Layer, Project Report for ME 3506, Advanced Fluid Mechanics I, El Paso, TX: Mechanical and Industrial Engineering Department, December 1983.
38. Martin Marietta Corp., Heliostat Field Wind Effects Tests, SAN/20422-2, San Francisco, CA: Department of Energy, February 1979.
39. Randall, D. E., D. D. McBride, and R. E. Tate, Steady-State Wind Loading on Parabolic Trough Solar Collectors, SAND 79-2134, Albuquerque, NM: Sandia National Laboratories, August 1980.
40. Randall, D. E., R. E. Tate, and D. A. Powers, Experimental Results of Pitching Moment Tests on Parabolic-Trough Solar-Collector Array Configurations, SAND 82-1569, Albuquerque, NM: Sandia National Laboratories, December 1982.
41. Sturrock, J. W., "Aerodynamic Studies of Shelterbelts in New Zealand," New Zealand Journal of Science, Vol. 12, No. 4, 1969.

42. Peterka, J. A., B. Bienkiewicz, and J. E. Cermak, Technical Feasibility of Innovative Concepts for Avoiding or Reducing Wind Loads on Concentrator Collectors - Task I Report for Solar Energy Research Institute, Fort Collins, CO: Colorado State University, March 1984.

DISTRIBUTION LIST

Kosta Achin
Sandia National Laboratories
Division 8473
P.O. Box 969
Livermore, CA 94550

R. E. Akins, Ph.D.
Professor, Engineering Science and
Mechanics
Virginia Polytechnic Institute and
State University
Blacksburg, VA 24061

Don Bartlett
Boeing Engineering and Construction
Company
Mail Stop 9A-42
P.O. Box 3707
Seattle, WA 98125

David Blake, Ph.D.
Engineering Manager
Acurex Corporation
485 Clyde Avenue
Mountain View, CA 94042

Floyd Blake
ARCO Ventures Company
7061 South University Blvd.
Littleton, CO 80122

John Cermak, Ph.D.
Professor, Civil Engineering
Dept. of Civil Engineering
Fluid Mech. and Wind Eng. Program
Colorado State University
Fort Collins, CO 80523

Bill Delemeter, Ph.D.
Sandia National Laboratories
Division 8453
P.O. Box 969
Livermore, CA 94550

William Dickhart
Assistant to the Director
The Budd Company
Fort Washington, PA 19034

Robert Gervais
McDonnell Douglas Company
5301 Bolsa Avenue
Huntington Beach, CA 92647

H. Gerwin, Ph.D.
Gerwin Research
14305 Anstead Road
Silver Spring, MD 20904

Roger Gillette
Boeing Engineering and Construction
Company
P.O. Box 3707
Seattle, WA 98125

Jim Leonard, Ph.D.
Sandia National Laboratories
Division 6227
P.O. Box 5800
Albuquerque, NM 87115

John Lucas, Ph.D.
Jet Propulsion Laboratory
4800 Oak Grove Drive
Pasadena, CA 94103

Monte McGlaum
LaJet Company
3131 Antilly Road
Abilene, TX 79605

Clayton Mavis
Sandia National Laboratories
Division 8473
P.O. Box 969
Livermore, CA 94550

Jon Peterka, Ph.D.
Professor, Civil Engineering
Dept. of Civil Engineering
Fluid Mech. and Wind Eng. Program
Colorado State University
Fort Collins, CO 80523

J. T. Pearson, Ph.D.
Purdue University
Mechanical Engineering Building
West Lafayette, IN 47907

Tim Reinhold, Ph.D.
Center for Building Technology
National Bureau of Standards
Washington, DC 202034

Bob Reuter, Ph.D.
Sandia National Laboratories
Division 1523
P.O. Box 5800
Albuquerque, NM 87115

Jim Rogan, Ph.D.
McDonnell Douglas Company
5301 Bolsa Avenue
Huntington Beach, CA 92647

T. W. Rogers
United Space Boosters
2-EO
P.O. Box 1626
Huntsville, AL 35807

E. J. Roshke, Ph.D.
The Jet Propulsion Laboratory
California Institute of Technology
4800 Oak Grove Drive
Pasadena, CA 91109

Aharon Roy
Head, Solar Power Laboratory
Department of Chemical Engineering
Ben-Gurion University of Negev
P.O. Box 653
Beer-Sheva 84105, ISRAEL

Dan Sallis
Dan-Ka Products
790 Umatilla
Suite 212
Denver, CO 80204

John Schaeffer, Ph.D.
Manager of Projects
Projects Department
Acurex Corporation
485 Clyde Avenue
Mountain View, CA 94042

Martin Scheve
Department of Energy
CE-314, Room 5H-041
Forrestal Building
1000 Independence Avenue, S.W.
Washington, DC 20585

Jeff Shingleton
49 Elm Avenue
Takoma Park, MD 20912

Jack Swearingen, Ph.D.
Sandia National Laboratories
Division 8453
P.O. Box 969
Livermore, CA 94550

H. Tielman, Ph.D.
Professor, Engineering Science and
Mechanics
Virginia Polytechnic Institute and
State University
Blacksburg, VA 24061

A. Thomas
Instrumentation and Services Unit
Indian Institute of Science
Bangalore - 560-012
INDIA

Kenell J. Touryan, Ph.D.
Vice President, R&D
Mt. Moriah Trust
6200 Plateau Drive
Englewood, CO 80111

Lee Weinstein
McDonnell Douglas Company
5301 Bolsa Avenue
Huntington Beach, CA 92647

Frank Wilkins
Department of Energy
CE-314, Room 5H-041
Forrestal Building
1000 Independence Avenue, S.W.
Washington, DC 20585

Document Control Page	1. SERI Report No. SERI/TR-253-2169	2. NTIS Accession No.	3. Recipient's Accession No.
4. Title and Subtitle Wind Loading on Solar Collectors		5. Publication Date June 1985	
		6.	
7. Author(s) S. Bhaduri and L.M. Murphy		8. Performing Organization Rept. No.	
9. Performing Organization Name and Address Solar Energy Research Institute 1617 Cole Boulevard Golden, Colorado 80401		10. Project/Task/Work Unit No. 1384.30 and 5102.31	
		11. Contract (C) or Grant (G) No. (C) (G)	
12. Sponsoring Organization Name and Address		13. Type of Report & Period Covered Technical Report	
		14.	
15. Supplementary Notes			
16. Abstract (Limit: 200 words) The present design methodology for the determination of wind loading on the various solar collectors has been reviewed and assessed. The total force coefficients of flat plates of aspect ratios 1.0 and 3.0, respectively, at various angles of attack obtained by using the guidelines of the ANSI A58.1-1982, have been compared with those obtained by using the methodology of the ASCE Task Committee, 1961, and the experimental results of the full-scale test of heliostats by Peglow. The turbulent energy spectra, currently employed in the building code, are compared with those of Kaimal et al., Lumley, and Ponofsky for wind velocities of 20.0 m/s and 40.24 m/s at an elevation of 9.15 m. The longitudinal spectra of the building code overestimates the Kaimal spectra in the frequency range of 0.007 Hz - 0.08 Hz and underestimates beyond the frequency of 0.08 Hz. The peak angles of attack, on the heliostat, stowed in horizontal position, due to turbulent vertical and lateral components of wind velocity, have been estimated by using Daniel's methodology for three wind velocities and compared with the value suggested by the code. The experimental results of a simple test in the laboratory indicate the feasibility of decreasing the drag forces of the flat plate by reducing the solidity ratio.			
17. Document Analysis a. Descriptors Dynamic Loads; Heliostats; Mechanical Structures; Solar Collectors; Stresses; Wind; Wind Loads b. Identifiers/Open-Ended Terms c. UC Categories 62e			
18. Availability Statement National Technical Information Service U.S. Department of Commerce 5285 Port Royal Road Springfield, Virginia 22161		19. No. of Pages 50	
		20. Price A03	